

Article

2-(2-(Dimethylamino)vinyl)-4*H*-pyran-4-ones as Novel and Convenient Building-Blocks for the Synthesis of Conjugated 4-Pyrone Derivatives

 Dmitrii L. Obydenov , Diana I. Nigmatova, Alexander S. Shirinkin , Oleg E. Melnikov, Vladislav V. Fedin , Sergey A. Usachev , Alena E. Simbirtseva, Mikhail Y. Kornev and Vyacheslav Y. Sosnovskikh 

Institute of Natural Sciences and Mathematics, Ural Federal University, 620000 Ekaterinburg, Russia

* Correspondence: dobydenov@mail.ru; Tel.: +7-343-3899597

Abstract: A straightforward approach for the construction of the new class of conjugated pyrans based on enamination of 2-methyl-4-pyrones with DMF-DMA was developed. 2-(2-(Dimethylamino)vinyl)-4-pyrones are highly reactive substrates that undergo 1,6-conjugate addition/elimination or 1,3-dipolar cycloaddition/elimination followed by substitution of the dimethylamino group without ring opening. This strategy includes selective transformations leading to conjugated and isoxazolyl-substituted 4-pyrone structures. The photophysical properties of the prepared 4-pyrones were determined in view of further design of novel merocyanine fluorophores. A solvatochromism was found for enamino-substituted 4-pyrones accompanied by a strong increase in fluorescence intensity in alcohols. The prepared conjugated structures demonstrated valuable photophysical properties, such as a large Stokes shift (up to 204 nm) and a good quantum yield (up to 28%).

Keywords: 4-pyrone; DMF-DMA; enamination; cycloaddition; merocyanine; 1,6-conjugate addition; solvatochromism; fluorophore


Citation: Obydenov, D.L.;

Nigmatova, D.I.; Shirinkin, A.S.; Melnikov, O.E.; Fedin, V.V.; Usachev, S.A.; Simbirtseva, A.E.; Kornev, M.Y.; Sosnovskikh, V.Y.

 2-(2-(Dimethylamino)vinyl)-4*H*-pyran-4-ones as Novel and Convenient Building-Blocks for the Synthesis of Conjugated 4-Pyrone Derivatives. *Molecules* **2022**, *27*, 8996. <https://doi.org/10.3390/molecules27248996>

Academic Editor: Joseph Sloop

Received: 20 November 2022

Accepted: 13 December 2022

Published: 16 December 2022

Publisher's Note: MDPI stays neutral with regard to jurisdictional claims in published maps and institutional affiliations.



Copyright: © 2022 by the authors. Licensee MDPI, Basel, Switzerland. This article is an open access article distributed under the terms and conditions of the Creative Commons Attribution (CC BY) license (<https://creativecommons.org/licenses/by/4.0/>).

1. Introduction

4-Pyrones are an important class of compounds that are widely distributed in nature, exhibiting various beneficial biological activities (e.g., phenoxan (Figure 1), which is active against HIV) [1,2] and are also used as multifunctional building blocks for organic synthesis [3–8]. On the other hand, the presence of conjugated double bonds in the pyrone structure makes it possible to consider these heterocycles in terms of attractive photophysical properties. Hispidin, as an important styryl pyrone, is responsible for bioluminescence in basidiomycete fungi in the result of oxidation [9,10], and Cyercene A is a photoactive protective agent in marine mollusks [11,12]. It has also been shown that styryl-substituted 4-pyrones find applications as fluorophores [13–19], exhibiting mechanochromism and solvatochromism based on the aggregation-induced emission enhancement (AIEE) phenomenon [16–18] and can act as molecular switches [19].

The introduction of an additional electron-withdrawing substituent into the C-4 position of the pyrone ring by means of the Knoevenagel reaction leads to one of the most popular merocyanines, DCM (Figure 1), and other 4-methylene-4*H*-pyrans, which have found wide application due to their important photophysical properties [20–24].

The major methods for the preparation of 2-vinyl-substituted 4-pyrones are based on the functionalization of the active methyl group based on the aldol condensation with aromatic aldehydes (Scheme 1) [13–19]. In addition, approaches are known that include the decarboxylative rearrangement of dehydroacetic acid derivatives [15] or the Horner-Wadsworth–Emmons reaction, which finds particular use in the synthesis of naturally occurring pyrans [1,12]. To the best of our knowledge, the transformation of 2,6-dimethyl-4-pyrone with DMF-DMA resulted in the monoamination product with

poor yield (5%) [24], whereas β -dimethylaminoacrolein aminal acetals led to 6-bis(4-dimethylaminoalka-1,3-dienyl)-4*H*-pyran-4-ones [13].

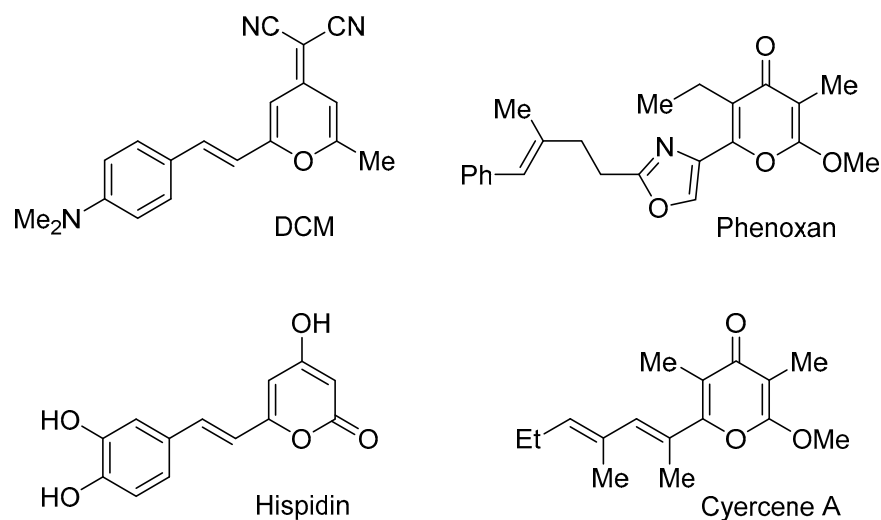
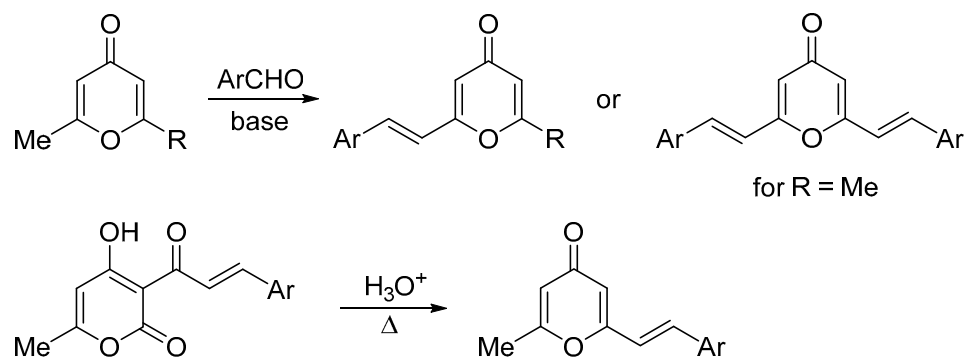
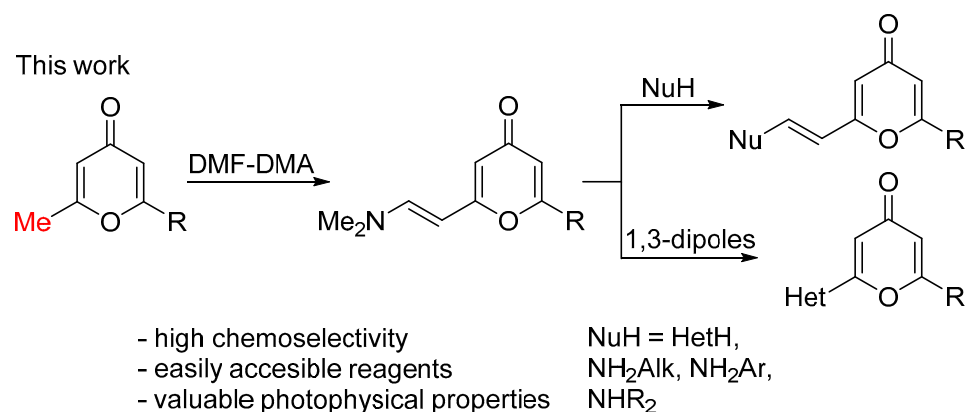


Figure 1. Some important 4-pyrones and their derivatives.

Previous work



This work



Scheme 1. General strategy for the synthesis of 2-vinyl-4-pyrones.

It is important to note that the methods for functionalizing 4-pyrones using nucleophilic reagents to create strong push-pull systems are scarcely studied. Typically, such reactions proceeded via ring opening transformation to form new cyclic systems [25–27]. The introduction of the enamino moiety [28–34] into 4-pyrone molecules leads to new highly reactive substrates, which can be used for the creation of valuable dyes via modification of 4-pyrone moiety or enamino group. Despite their attractiveness, 4-pyrone-based fluorophores are severely limited and have been described in just a few papers [13–19] due

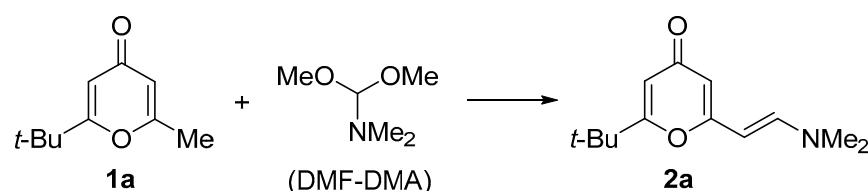
to the modest photophysical properties of the heterocycles and being overshadowed by derived dyes, 4-methylene-4*H*-pyrans.

In this paper, we describe a general strategy to 4-pyrone-bearing merocyanines based on an enamination with DMF-DMA and subsequent transformation of the dimethylaminovinyl group via a nucleophilic 1,6-addition or cycloaddition reaction. This approach opens straightforward access to a wide range of new promising pyran fluorophores.

2. Results and Discussion

2.1. Synthesis of 2-Enamino-substituted 4-Pyrones and Their Chemical Properties

The functionalization of the pyrone ring was carried out via an enamination reaction at the active methyl group using DMF-DMA as a reagent and a solvent (Scheme 2) [35]. *N*-Methylimidazole (NMI) was selected as a convenient base for the promotion of the transformation [36]. Enamination of 2-(*tert*-butyl)-6-methyl-4*H*-pyran-4-one (**1a**) with DMF-DMA (3 equiv.) and NMI (3 equiv.) at 100 °C in an autoclave afforded enamino-substituted 4-pyrone **2a** in only 15% yield (Table 1, entry 1). We decided to increase the reaction temperature to 120 °C and study the influence of the base amount on both the reaction outcome and time (TLC monitoring). When one equivalent of NMI was used, the reaction was completed in 15 h and the product was prepared in 40% yield (entry 2). We found that a further decrease in the amount of NMI (0.25–0.5 equivalent) allowed the improvement of the enamination reaction outcome until 67–72%, but it required longer heating (20–25 h) (TLC monitoring) (entries 3,4). The best yield (72%) of pyrone **2a** was achieved using 0.25 equivalents of *N*-methylimidazole though it took 25 h (entry 4). The isolation of the pyrone included simple recrystallization from *n*-heptane. Interestingly, the reaction also occurred without promotion of the base and gave the product in a lower yield (57%) under heating at 120 °C for 25 h (entry 5). Increasing temperature to 130 °C led to pyrone **2a** in 54% yield (entry 6). The enamination with the use of pyridine as a solvent and DMF-DMA (1.2 equiv.) at 100 °C or 120 °C did not produce the desired product.

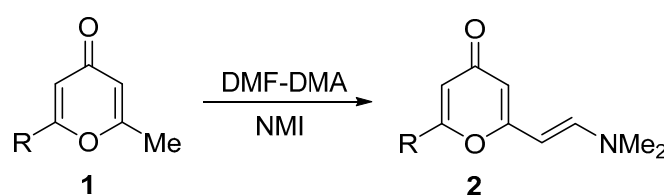


Scheme 2. Reaction of pyrone **1a** with DMF-DMA.

Table 1. Reaction condition optimization for the enamination of **1a**.

Entry	NMI, equiv.	Time, h	Temp., °C	Yield of 2a , %
1	3	8	100	15
2	1	15	120	40
3	0.5	20	120	67
4	0.25	25	120	72
5	–	25	120	57
6	0.25	10	130	54

The enamination reaction conditions were extended for various 2-methyl-4-pyrones (Scheme 3, Table 2), but this transformation turned out to be very sensitive to the nature of substituents at the pyrone ring. The enamination of 2-methyl-6-phenyl-4-pyrone (**1b**) with DMF-DMA proceeded for 12 h under the optimized conditions; as a result, pyrone **2b** was obtained in 53% yield. However, the reaction of 2-methyl-6-trifluoromethyl-4-pyrone (**1c**) was completed in 5 h at 120 °C, leading to the desired product in only low yield (12%). This result can be explained by side processes due to the presence of the trifluoromethyl group and high CH-acidity). Lowering the temperature to 100 °C made it possible to increase the yield up to 43%.



Scheme 3. Enamination of pyrones 1.

Table 2. The scope of enamino-substituted 4-pyrones 2.

Entry	R	Product	Temp., °C	Equiv. of NMI	Time, h	Yield, %
1	<i>t</i> -Bu	2a	120	0.25	15	72
2	Ph	2b	120	0.25	12	53
3	CF ₃	2c	100	0.25	5	43, 12 ^a
4	CO ₂ Me	2d	120	4	6	27 ^b , 8 ^c
5	PhCH = CH	2e	100	0.25	4	22
6	4-Me ₂ NC ₆ H ₄ CH = CH	2f	120	3	3	72
7	4-MeOC ₆ H ₄ CH = CH	2g	120	3	3	51

^a The reaction was carried out with 1.2 mmol of **1c** at 120 °C for 5 h in the presence of NMI (24.6 mg, 0.3 mmol) and DMF-DMA (429.0 mg, 3.6 mmol). ^b From ethyl 6-methylcomanate (**1d'**). ^c The reaction was carried out with methyl 6-methylcomanate (**1d**) at 120 °C for 4 h in the presence of NMI (24.6 mg, 0.3 mmol) and DMF-DMA (429.0 mg, 3.6 mmol).

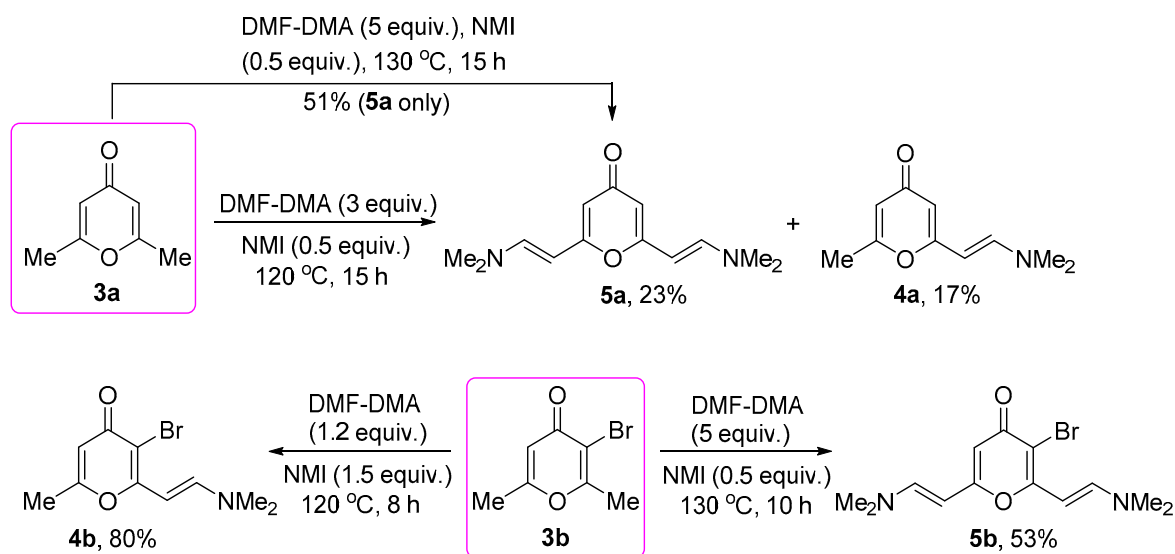
It was found that the enamination of ethyl 6-methylcomanate (**1d'**) with DMF-DMA and an excess of NMI (3 equiv.) at 120 °C was accompanied by the transesterification reaction to produce product **2d** in 27% yield (Scheme 3 Table 2). It is interesting to note that direct enamination of methyl 6-methylcomanate (**1d**) at 100 °C in the presence of NMI (0.25 equiv.) led to the desired product **2d** in only 8% yield.

We tried to extend the enamination on 2-methyl-6-styryl-4-pyrones **1e–g** for the synthesis of unsymmetrical 2,6-divinyl-4-pyrones **2e–g** (Table 2). The reaction of 2-methyl-6-styryl-4-pyrone (**1e**) at 120 °C with a threefold excess of DMF-DMA and different amounts of *N*-methylimidazole did not lead to the desired product. Lowering the temperature to 100 °C made it possible to obtain product **2e** in 22% yield for 4 h (TLC monitoring). For starting 2-methyl-6-styryl-4-pyrones **1f,g**, the use of the optimized conditions did not give the desired products because of low solubility of the starting materials. The enamination of pyrones **1f,g** with threefold excess of *N*-methylimidazole and heating at 120 °C for 3 h led to complete conversion of the starting 4-pyrone, and products **2f,g** were isolated by the treatment with diethyl ether in 72 and 51% yields, respectively. Such a difference in the behavior of styrylpyrones may be connected with the presence of electron-donating substituents, which deactivated the double bond of the styryl fragment and reduced the possibility of side reactions.

The reaction of 2,6-dimethyl-4-pyrone **3a** with three equivalent DMF-DMA and 0.5 equiv. of NMI was carried out at 120 °C for 15 h, resulting in a mixture of products of enamination **4a** and **5a** (Scheme 4). Recrystallization from *n*-heptane easily allowed the separation of pyrones **4a** and **5a** and isolation them in pure form in 17% and 23% yields, respectively. All our attempts to carry out more selective mono-enamination by lowering the temperature, variation of reagent amounts, and increasing the reaction time were unsuccessful and accompanied by incomplete conversion and the formation of the bis(enamino) derivative, which did not allow the preparation of product **4a** in pure form directly.

The use of an excess of DMF-DMA (5 equiv.) and heating at 130 °C for 15 h made it possible to increase the yield of bisenamine **5a** to 51%. At the same time, the formation of mono-enamino derivative **4a** was not observed. Carrying out the reaction without using NMI or using one equivalent of NMI resulted in product **5a** in 41 and 45% yields, respectively. The transformation of 3-bromo-2,6-dimethyl-4-pyrone (**3b**) led to a double enamination product **5b** in 53% yield. This result can probably be explained by a higher CH-acidity of the methyl groups. We also managed to carry out mono-enamination selectively at the methyl group located near the electron-withdrawing bromine atom, and

pyrone **4b** was prepared in high yield (80%) (Scheme 4). The structure of the product was assigned on the basis of the chemical shift of the methyl group in comparison with the starting 2,6-dimethyl-3-bromo-4-pyrone (**3b**) and product **4b**.



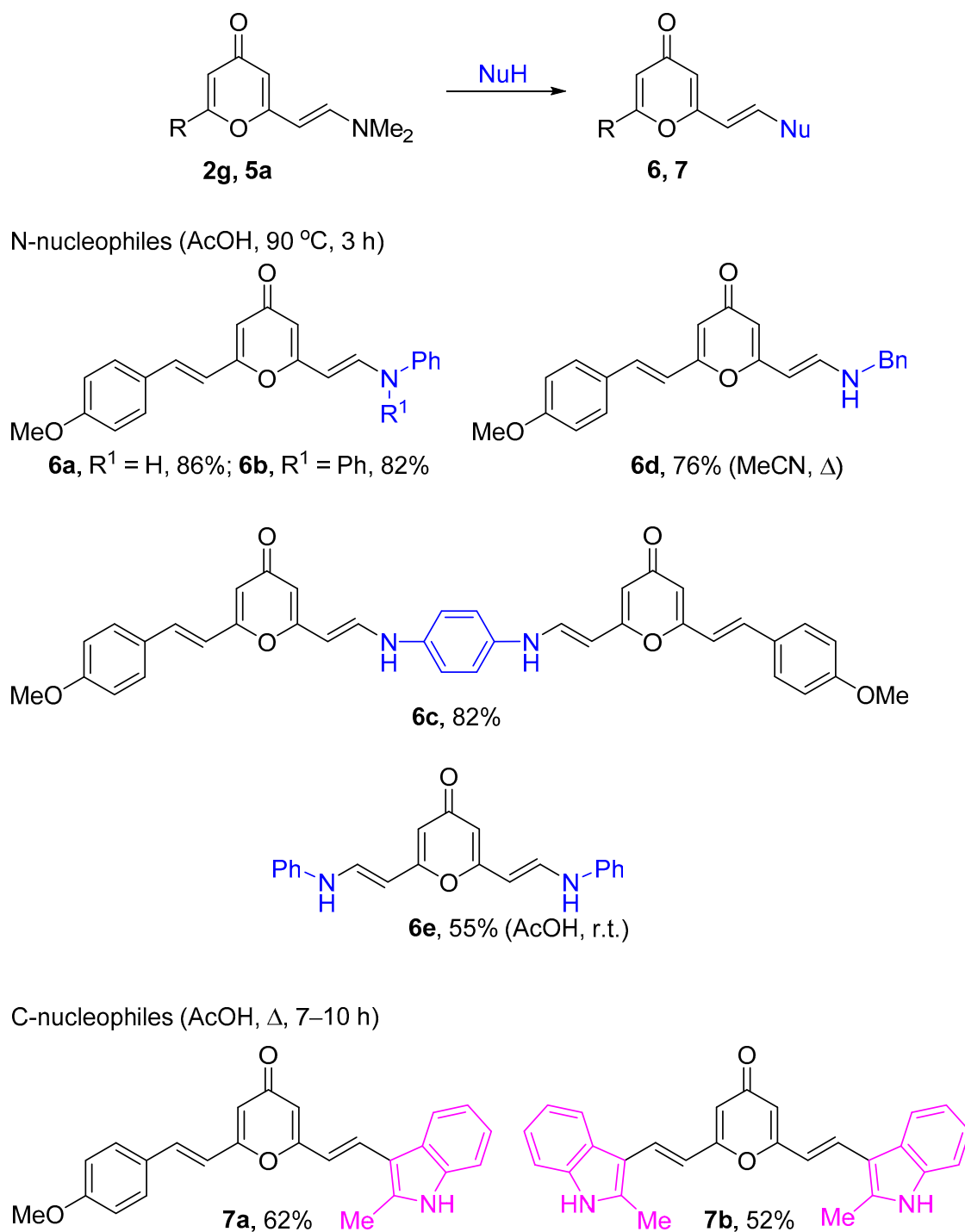
Scheme 4. Enamination of 2,6-dimethyl-4-pyrones **3a,b**.

The ^1H NMR spectra of the obtained dimethylamino-substituted pyrones **2,4,5** demonstrate a characteristic set of two doublets of the enamino group with 3J coupling of 12.6–13.3 Hz, which indicates the *E*-configuration of the double bond and its partially double order due to the strong push-pull nature [31,36].

To study the chemical properties of mono-enamino-substituted 4-pyrones **2** with various nucleophilic reagents, compound **2g** was used as an example to obtain conjugated structures (Scheme 5). We found that heating in AcOH turned out to be convenient conditions for carrying out the reactions. The transformation of pyrone **2g** with aniline or diphenylamine at 90 °C led to the substitution of the dimethylamino group and the formation of products **6a,b** in 82–86% yield. The reaction of substance **2g** with *p*-phenylenediamine as a binucleophile gave product **6c** as the result of an attack on both amino groups. It was found that pyrone **2g** reacted with benzylamine under reflux in acetonitrile to form product **6d** in 76% yield. The transformation of bis(enamino)pyrone **5a** with aniline was found to proceed at room temperature, leading to product **6e** in 55% yield. Thus, it has been shown that the side chain of γ -pyrone can easily be functionalized with aliphatic and aromatic amines.

Enamino-substituted pyrones **2g** and **5a** were able to react with 2-methylindole as a C-nucleophile to form indolyl-substituted 4-pyrones **7a,b** in 52–62% yields under reflux in AcOH for 7–10 h (Scheme 5). The transformation of bis(enamino)pyrone **5a** with 2-methylindole included the substitution at two enamino fragments and led to bis(indolylvinyl)-4-pyrone **7b** in 52% yield.

Next, we investigated the cycloaddition of enamino-substituted 4-pyrones with 1,3-dipoles (Scheme 6). It was observed that organic azides and diphenylnitrilimine did not give the desired products, which is probably due to the electron-withdrawing properties of the pyrone ring. The reaction with benzonitrile oxide, which was generated in situ from *N*-hydroxybenzimidoyl chloride [25], in dioxane without the use of a base led to the formation of isoxazolyl-substituted 4-pyrones in 39–80% yields. Although compounds **2f,g** bear two double bonds of different nature, the transformation proceeded chemoselectively at the enamino fragment. In the case of bis(enamino) derivative **5a**, the cycloaddition occurred at both enamino moieties to give 2,6-bis(isoxazolyl)-4-pyrone **9** in 39% yield.



Scheme 5. Reactions of enamino-substituted 4-pyrones **2g** and **5a** with nucleophiles.

2.2. Photophysical Properties of Products

For the series of enamino-substituted 4-pyrones, the photophysical properties were studied to assess the prospects for their use as fluorophores. We started with the study of the influence of the nature of the solvent on the absorption and emission spectra of (*E*)-2-(2-(dimethylamino)vinyl)-6-methyl-4*H*-pyran-4-one (**4a**) and 2,6-bis((*E*)-2-(dimethylamino)vinyl)-4*H*-pyran-4-one (**5a**).

For the monoenamino-substituted compound **4a**, the absorption spectrum includes one-band at 334–363 nm with an extinction coefficient of 29,200–35,900 M⁻¹cm⁻¹ (Figure 2, Table 3). In aprotic solvents, the absorption maximum is observed at 334–350 nm. For alco-

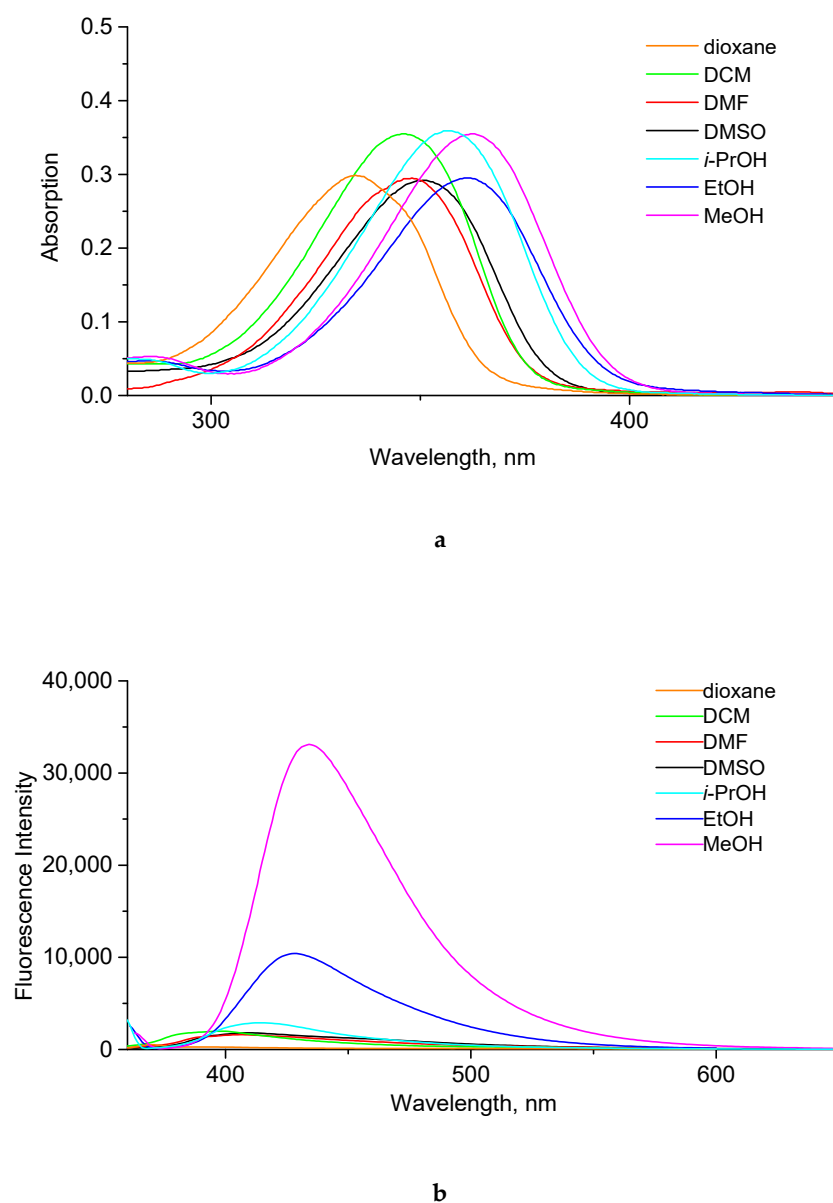


Figure 2. Absorption (a) and emission (b) spectra of compound **4a** in various solvents ($C = 1.0 \times 10^{-5}$ M).

Table 3. Absorption and fluorescence spectral data of compound **4a** in various solvents ($C = 1.0 \times 10^{-5}$ M).

Compound	Solvent	$\lambda_{\text{abs}}, \text{nm}^a$	$\lambda_{\text{em}}, \text{nm}^b$	$\epsilon, \text{M}^{-1}\text{cm}^{-1}$	Stokes Shift, nm	QY, % ^c
 4a	dioxane	334	370	29,900	26	<0.1 ^d
	CH ₂ Cl ₂	345	399	35,500	54	<0.1
	DMF	348	407	29,500	59	<0.1
	DMSO	350	408	29,200	58	0.2
	<i>i</i> -PrOH	356	415	35,900	59	0.3
	EtOH	361	428	29,500	67	1.4
	MeOH	363	434	35,500	71	3.6

^a Absorption maximum wavelength. ^b Excitation wavelength corresponds to λ_{abs} . ^c The relative fluorescence quantum yield (QY) was estimated using the solution of rhodamine 6G in ethanol as a standard (QY_{std} = 94%, λ_{ex} = 480 nm) according to the described method [35]. ^d The relative fluorescence quantum yield (QY) was estimated using a 0.1 M H₂SO₄ solution of quinine sulfate solution (QY_{std} = 54%, λ_{ex} = 360 nm) according to the described method [37].

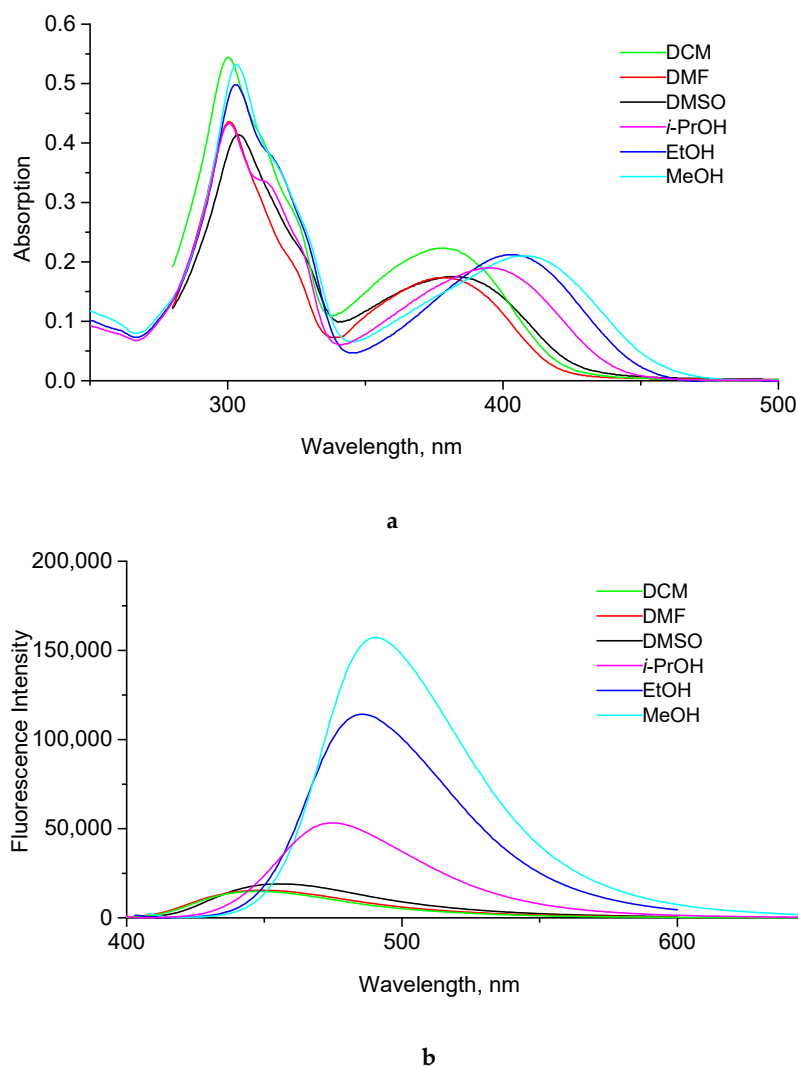
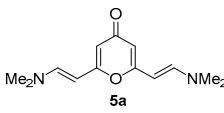


Figure 3. Absorption (a) and emission (b) spectra of compound **5a** in various solvents ($C = 1.0 \times 10^{-5}$ M).

Table 4. Absorption and fluorescence spectral data of compound **5a** in various solvents ($C = 1.0 \times 10^{-5}$ M).

Compound	Solvent	$\lambda_{\text{abs}}, \text{nm}^a$	$\lambda_{\text{em}}, \text{nm}^b$	$\epsilon, \text{M}^{-1}\text{cm}^{-1}$	Stokes Shift, nm	QY, % ^c
 5a	CH ₂ Cl ₂	300	447	54,400	69	3.0
		378		22,300		
	DMF	300	450	43,600	72	4.1
		378		17,400		
	DMSO	304	455	41,400	74	2.3
		381		17,500		
	<i>i</i> -PrOH	301	475	43,300	80	11
		395		19,000		
	EtOH	303	485	49,800	82	21
		403		21,200		
	MeOH	303	490	53,200	83	28
		408		21,000		

^a Absorption maximum wavelengths. ^b Excitation wavelength corresponds to λ_{abs} . ^c The relative fluorescence quantum yield (QY) was estimated using the solution of rhodamine 6G in ethanol as a standard (QY_{std} = 94%, λ_{ex} = 480 nm) according to the described method [37].

For the design of new fluorophores, we studied a number of functionalized enamino-substituted 4-pyrones (Figure 4, Table 5). The introduction of the *tert*-butyl group, compared to the methyl group, has practically no effect on the photophysical properties. The absorption and emission spectra of (*tert*-butyl)-6-(2-(dimethylamino)vinyl)-4*H*-pyran-4-one (**2a**) are very similar for monoamine derivative **4a**. The introduction of the phenyl group complicates the absorption spectrum, as a result, several maxima are observed. In this case, the major absorption maximum appears at 380 nm with an extinction coefficient of $19,700 \text{ M}^{-1}\text{cm}^{-1}$. An important feature of fluorescence is the large Stokes shift, which amounts to 147 nm (QY = 3.4%). For dimethylenamino derivative **2f** bearing the *p*-dimethylaminostyryl moiety, the absorption spectra show several maxima with approximately the same value of the extinction coefficient. The fluorescence spectrum exhibits one-band emission at 572 nm ($\lambda_{\text{ex}} = 368 \text{ nm}$), which is characterized by higher quantum yield (18%) and a significant Stokes shift (204 nm). Similarly, the *p*-MeO-styryl-substituted compound **2g** has several bands with low intensity in absorption spectra and very weak fluorescence emission.

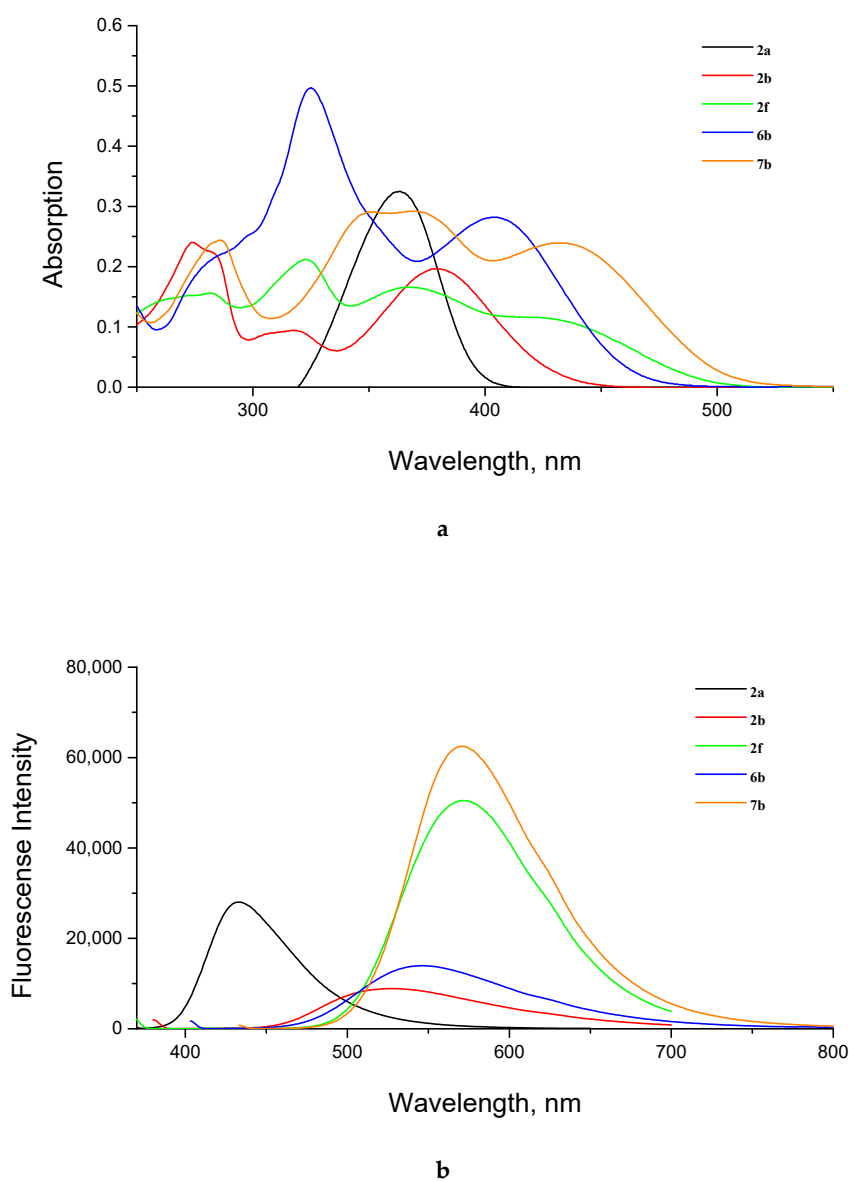
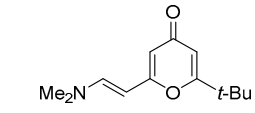
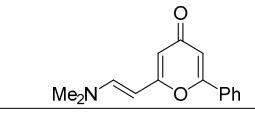
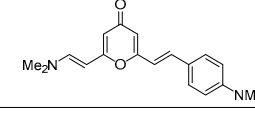
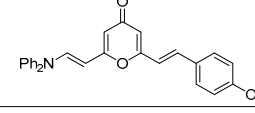
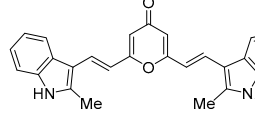


Figure 4. Absorption (a) and emission (b) spectra of compounds **2a,b,f**; **6b**; and **7b** in MeOH ($C = 1.0 \times 10^{-5} \text{ M}$).

Table 5. Absorption and fluorescence spectral data of compounds **2a,b,f**; **6b**; and **7b** in MeOH (C = 1.0 × 10^{−5} M).

Compd.	Structure	$\lambda_{\text{abs}},$ nm ^a	$\lambda_{\text{em}},$ nm ^b	$\epsilon, \text{M}^{-1} \text{cm}^{-1}$	Stokes Shift, nm	QY, % ^c
2a		364	433	32,500	70	3.0
2b		274		24,000		
		317		9400		
		380	527	19,700	147	3.4
2f		323		21,200		
		368	572	16,600	204	18
6b		325		49,700		
		404	546	28,200	142	3.4
7b		286		24,400		
		375–348 (plateau)		29,000		
		433	571	23,900	138	15

^a Absorption maximum wavelengths. ^b Excitation wavelength corresponds to λ_{abs} . ^c The relative fluorescence quantum yield (QY) was estimated using the solution of rhodamine 6G in ethanol as a standard (QY_{std} = 94%, λ_{ex} = 480 nm) according to the described method [37].

Introduction of the diphenylamino substituent allows the improvement of photophysical properties. Thus, for *p*-MeO-styryl derivative **6b**, two intense maxima are found in the absorption spectrum at 404 nm and 350 nm. This substance shows one maximum in the emission spectrum at 546 nm (λ_{ex} = 368 nm) and a quantum yield of 3.4%. Next, the bis(indolyl) derivative **7b** was investigated as a symmetrical compound with an extended conjugation system. Its absorption spectrum (MeOH) contains a major maximum at 433 nm, a plateau in the range of 375–348 nm, and a minor maximum at 286 nm. The emission spectrum contains one band at 571 nm, while the quantum yield reaches 15%.

2.3. Theoretical Calculations of the Absorption and Emission

We performed a DFT/TD-DFT quantum chemical calculations of absorption/emission maxima for representative compounds **4a** and **5a** in vacuo and in solvated phase (DMSO, EtOH, and MeOH) using the conductor-like polar continuum model (C-PCM). In the series of the ground state (GS), the first singlet excited state (S_1) optimizations were made and the energies of the first seven Franck-Condon singlet states were computed. All calculations were carried out at the (TD-)DFT (CAM-)B3LYP/6-31++G** level of theory for the most stable *s-trans* conformations [13]. Results of this calculations are provided in Table 6; the optimized geometries of GS and S_1 are listed in Supplementary Materials.

The optimizations of the ground state (GS) geometry revealed that both molecules have a planar structure of D- π -A conjugation chains. Calculated Stokes shift values in a solvated phase were 27–30 nm for 2-(2-(dimethylamino)vinyl)-6-methyl-4-pyrone (**4a**) and 92–103 nm for 2,6-bis(2-(dimethylamino)vinyl)-4-pyrone (**5a**), which are in agreement with the experimental Stokes shifts. Also, in all solvents the dipole moment values increased under excitation to S_1 . On the base of Franck-Condon (FC) excitations and S_1 optimized geometries energies and their oscillator strengths, we plotted theoretical absorption and emission spectra (See Supplementary Materials Figures S1–S6, absorption/emission maxima are also provided in Table S6). Because the DFT usually overestimates long-wavelength

polymethine transitions, all calculated maxima are notably blue-shifted compared to the experimental ones [38]. According to TD-DFT calculations of S_1^{FC} – S_7^{FC} states in all solvents, the most intense absorption corresponds to $\pi \rightarrow \pi^*$ transition and $S_0 \rightarrow S_1$ from the highest occupied molecular orbital (HOMO) to the lowest unoccupied molecular orbital (LUMO) for compound **4a**, whereas $S_0 \rightarrow S_2$ (HOMO–1 \rightarrow LUMO) transition prevails for compound **5a** (Table 6). In the case of compound **5a**, the $S_0 \rightarrow S_1$ transition is less intense ($f_{GS} = 0.527$ for MeOH) and redshifted ($\lambda_{abs} = 376$ nm for MeOH), which agrees well with the experimental absorption spectrum demonstrating double bands.

Table 6. Calculated absorption and emission properties of **4a** and **5a** in vacuo, DMSO, EtOH, and MeOH ^a.

Entry	Compd.	Solvent	λ_{abs}, nm	f_{GS}	λ_{em}, nm	f_{S1}	μ_{GS}, D	μ_{S1}, D	$\mu_{(GS \rightarrow S1)}, \text{D}$
1	4a	Vacuum	286	0.718	293 ^b	0.744 ^b	8.808	4.246	–4.562
2		DMSO	331	1.070	361	1.092	0.097	3.114	3.017
3		EtOH	340	1.072	367	1.082	1.102	4.372	3.270
4		MeOH	342	1.076	369	1.086	1.246	4.407	3.161
5	5a	Vacuum	252	0.631	315	0.363	10.772	13.084	2.312
6		DMSO	302	1.891	394	0.507	0.190	2.386	2.196
7		EtOH	307	1.903	408	0.529	1.407	3.882	2.475
8		MeOH	308	1.921	411	0.537	1.556	4.033	2.477

^a λ_{abs} —absorption maximum, f_{GS} —oscillator strength for the absorption maximum, λ_{em} —emission maximum, f_{S1} —oscillator strength for the emission maximum, μ_{GS} , μ_{S1} —dipole moments of GS and S_1 optimized geometries, $\mu_{(GS \rightarrow S1)}$ —the difference in dipole moments of GS and S_1 . ^b Data provided for S_2 , since S_1 (339 nm, 3.662 eV) has oscillator strength very close to zero.

To explain the strong influence of alcohols on fluorescence, the charges on the carbonyl oxygen of pyrones **4a** and **5a** in the ground and excited states were compared. An increase in the electron density on oxygen can cause its specific solvation due to the formation of hydrogen bonds, leading to the improvement of the fluorescence properties. The charge of pyrone **5a** bearing two electron-donating substituents is in all cases higher than that of pyrone **4a** in the corresponding solvent, which can be explained by the stronger push-pull nature of the former. In addition, the maximum negative charge was found in EtOH and MeOH, both in the ground (–0.731 and –0.746 for **4a**; –0.758 and –0.776 for **5a**) and excited (–0.823 and –0.839 for **4a**; –0.905 and –0.925 for **5a**) states (Table 7). For all excited states, an increase in the negative charge on carbonyl oxygen is observed (except for **4a** in vacuum), which is in good agreement with the change in dipole moments. The strongest charge changes during the $GS \rightarrow S_1$ transition were found in MeOH (0.093 for **4a**, 0.149 for **5a**). This result is related to the ICT effect in this solvent, which is more pronounced for pyrone **5a** and determines the stabilization of the excited states via the hydrogen bonding interaction between the carbonyl group and alcohol molecules [39]. Besides, the ICT phenomena for the pyrones were confirmed with the use of electron density difference (EDD) maps (See Supplementary Materials Figures S7–S10).

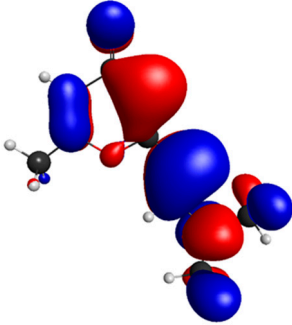
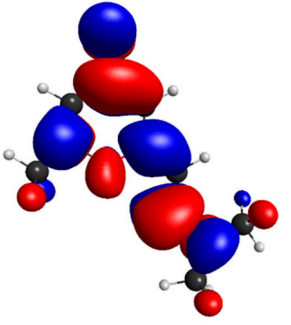
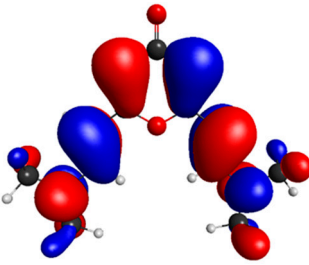
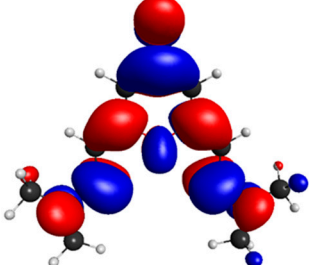
Table 7. Mulliken charges at the carbonyl oxygen atom of pyrones **4a** and **5a**.

Entry	Compd.	Charge	Vacuum	DMSO	EtOH	MeOH
1	4a	GS	–0.537	–0.640	–0.731	–0.746
2		S_1	–0.303	–0.711	–0.823	–0.839
3		$\Delta(GS-S_1)$	–0.234	0.071	0.092	0.093
4	5a	GS	–0.549	–0.660	–0.758	–0.776
5		S_1	–0.634	–0.779	–0.905	–0.925
6		$\Delta(GS-S_1)$	0.085	0.119	0.147	0.149

The analysis of the frontier MOs for the ground states in the solvents (DMSO, MeOH, EtOH) and the gas phase showed that both HOMO and LUMO frontier orbitals are localized

chiefly on the polymethine chain atoms, which is known to be typical for merocyanine dyes [22] (Table 8, See Supplementary Materials Tables S1–S8). Opposite to mono(enamino) derivative **4a**, bis(enamino) derivative **5a** exhibited a complete absence of the electron density at the carbonyl moiety of the conjugation chain for the HOMO, whereas the LUMO localization involves the whole π -conjugation, indicating the ICT effect under excitation. This feature can be connected with a large Stokes shift of bis(enamino) derivative **5a** and the red-shifted emission compared to **4a**.

Table 8. Ground state frontier orbitals of compounds **4a** and **5a** in MeOH ^a.

Entry	Compound	HOMO	LUMO
1	4a	 −5.36 eV	 −1.36 eV
2	5a	 −5.06 eV	 −1.41 eV

^a Isosurfaces correspond to 0.02 psi/0.0004 rho).

Thus, a convenient method of 4-pyrone functionalization is developed via enamination of 2-methyl-4-pyrones with DMF-DMA. Enamino-substituted 4-pyrones were able to react with nucleophiles and 1,3-dipoles with the substitution of the dimethylamino group and the formation of conjugated push-pull and isoxazolyl-substituted 4-pyrones, respectively. The transformations occurred with high chemoselectivity without 4-pyrone ring opening and provided a convenient platform for the synthesis and design of 4-pyrone-based fluorophores. For the first time, the solvatochromism of 4-pyrones in protic solvents due to specific solvation was discovered, leading to a strong increase in the fluorescence intensity compared to aprotic solvents. 4-Pyrones bearing two enamino fragments show a higher quantum yield and significant Stokes shift, which can be explained by their stronger push-pull character. The prepared pyrone merocyanines are of interest due to attractive photophysical properties and easy modification of the conjugated chain, which can contribute to the development of the synthesis of new organic fluorophores.

3. Materials and Methods

NMR spectra were recorded on Bruker DRX-400 (Bruker BioSpin GmbH, Ettlingen, Germany, work frequencies: ¹H, 400 MHz; ¹³C, 101 MHz; ¹⁹F, 376 Hz), Bruker Avance-400 (Bruker BioSpin GmbH, Rheinstetten, Germany, work frequencies: ¹H, 400 MHz; ¹³C, 101 MHz), Bruker Avance III-500 (Bruker BioSpin GmbH, Rheinstetten, Germany, work frequencies: ¹H, 500 MHz; ¹³C, 126 MHz), and Bruker Avance NEO (Bruker BioSpin GmbH,

work frequencies: ^1H , 600 MHz; ^{13}C , 151 MHz) spectrometers in DMSO- d_6 or CDCl_3 . The chemical shifts (δ) are reported in ppm relative to the internal standard TMS (^1H NMR), C_6F_6 (^{19}F NMR), and residual signals of the solvents (^{13}C NMR). IR spectra were recorded on a Shimadzu IRSpirit-T (Shimadzu Corp., Kyoto, Japan) spectrometer using an attenuated total reflectance (ATR) unit (FTIR mode, diamond prism); the absorbance maxima (ν) are reported in cm^{-1} . Electron absorption spectra were obtained with a Shimadzu UV-1900 (Shimadzu Corp.) spectrophotometer; fluorescence spectra were obtained with a Shimadzu RF-6000 (Shimadzu Corp.) fluorescence spectrophotometer.

Mass spectra (ESI-MS) were measured with a Waters Xevo QToF instrument (Waters Corp., Milford, MA, USA). Elemental analyses were performed on an automatic analyzer PerkinElmer PE 2400 (Perkin Elmer Instruments, Waltham, MA, USA). Melting points were determined using a Stuart SMP40 melting point apparatus (Bibby Scientific Ltd., Stone, Staffordshire, UK). Column chromatography was performed on silica gel (Merck 60, 70–230 mesh). All solvents used were dried and distilled by standard procedures. 2-Methyl-6-styryl-4-pyrones [15], esters of 6-methyl-4-pyrone-2-carboxylic acid [40,41], 2-*tert*-butyl-6-methyl-4-pyrone [42], and 2-methyl-6-phenyl-4-pyrone [42] were prepared according to the literature procedure.

3.1. Quantum Mechanical Calculations

The ground state molecular geometry of the compounds under investigation was fully optimized at density functional theory (DFT) level, both in vacuo and in the solvated phase (DMSO, EtOH, MeOH). For all geometry optimizations, the B3LYP hybrid functional [43] coupled with the 6-31G(d,p)++ basis set was chosen. Solvent effects were taken into account via the implicit conductor-like polarizable continuum model (C-PCM). For the evaluation of energetics, Solvation Model Density (SMD) parametrization was employed [44]. The vibrational frequencies and thermochemicals were computed in harmonic approximation at $T = 298.15$ K and $p = 1$ atm, and no imaginary frequencies were found.

The UV-vis absorption spectra for the equilibrium geometries were calculated at time-dependent density functional theory (TD-DFT) level, accounting for $S_0 \rightarrow S_n$ ($n = 1$ to 7). The nature of the vertical excited electronic state was analyzed both in vacuo and in the solvated phase.

The first singlet excited state (S_1) geometry was optimized using analytical gradients and the first transitions $S_1 \rightarrow S_0$ of the emission. Properties of the excited states were calculated using the long-range corrected functional CAM-B3LYP [45,46] coupled with the 6-31G(d,p)++ basis set. The non-equilibrium solvation regime was set for vertical excited states calculations in the solvent phase, whereas the equilibrium solvation was used for adiabatic ones. All calculated UV-vis spectra were plotted as Gaussian curves with wavelengths of absorption/emission maxima as an expected value and $\sigma = 0.4$ eV.

The integration grid for the calculations was set to 96 radial shells and 302 angular points.

The RMS gradient convergence tolerance was set to 10^{-7} Hartree/Bohr for GS optimizations and to 10^{-5} Hartree/Bohr for S_1 optimizations. The density matrix convergence threshold for the self-consistent field was set to 10^{-5} a.u. for all DFT and to 10^{-6} a.u. for all TD-DFT optimizations.

All calculations were performed using the US GAMESS (ver. 30 September 2021, R2 Patch 1) software package for Linux x64 [47]. Frontier MOs were plotted with MacMolPlt software (ver. 7.7) [48]. Electron density difference maps were calculated with the use of Multiwfn v3.8 [49].

3.2. Synthesis of Compounds 2

Corresponding 4-pyrone **1** (1.2 mmol) was heated with DMF-DMA (429.0 mg, 3.6 mmol), *N*-methylimidazole (0.3 mmol for **2a–c,e**; 4.8 mmol for **2d**; 3.6 mmol for **2f,g**) in an autoclave at 100 °C (for **2c,e**) or 120 °C (for **2a,b,d,f,g**) for the needed time. For pyrones **2a–c**, the reaction mixture was treated by boiling *n*-heptane (40 mL). The solvent was decanted and

evaporated to 2 mL, and the solid was filtered. For products **2d,f,g**, the reaction mixture was treated with Et₂O and the solid that formed was filtered. Pyrone **2e** was isolated by flash-chromatography with the use of CHCl₃ as an eluent.

(*E*)-2-(*Tert*-butyl)-6-(2-(dimethylamino)vinyl)-4*H*-pyran-4-one (**2a**). The reaction was carried out for 15 h. Yield 191.2 mg (72%), yellow powder, mp 128–130 °C. IR (ATR) ν 2962, 2907, 2870, 1639, 1564, 1386, 1364, 1104. ¹H NMR (500 MHz, DMSO-*d*₆) δ 1.23 (9H, s, *t*-Bu), 2.90 (6H, br.s, NMe₂), 4.82 (1H, d, *J* = 13.2 Hz, =CH(α)), 5.62 (1H, d, *J* = 2.1 Hz, CH), 5.77 (1H, d, *J* = 2.1 Hz, CH), 7.26 (1H, d, *J* = 13.2 Hz, =CH(β)). ¹³C NMR (126 MHz, CDCl₃) δ 28.1, 35.8, 40.8 (br.s. NMe₂), 88.0, 104.8, 108.9, 144.8, 165.8, 172.8, 180.5. Anal. Calculated for C₁₃H₁₉NO₂: C 70.56; H 8.65; N 6.33. Found: C 70.58; H 8.76; N 6.33.

(*E*)-2-(2-(Dimethylamino)vinyl)-6-phenyl-4*H*-pyran-4-one (**2b**). The reaction was carried out for 12 h. Yield 153.5 mg (53%), yellow powder, mp 200 °C (destr.). IR (ATR) ν 3056, 2910, 1627, 1539, 1381, 1349, 1101. ¹H NMR (400 MHz, DMSO-*d*₆) δ 2.95 (6H, s, NMe₂), 4.92 (1H, d, *J* = 13.3, =CH(α)), 5.78 (1H, d, *J* = 2.2 Hz, H-3), 6.61 (1H, d, *J* = 2.2 Hz, H-5), 7.47 (1H, d, *J* = 13.3 Hz, =CH(β)), 7.52 (3H, m, Ph), 7.94 (2H, m, H-2, H-6 Ph). ¹³C NMR (101 MHz, DMSO-*d*₆) δ 86.9, 104.3, 110.1, 126.1, 129.4, 131.1, 132.0, 146.7, 160.4, 166.3, 178.3 (NMe₂ was not observed). HRMS (ESI) *m/z* [M + H]⁺. Calculated for C₁₅H₁₆NO₂: 242.1189. Found: 242.1103.

(*E*)-2-(2-(Dimethylamino)vinyl)-6-(trifluoromethyl)-4*H*-pyran-4-one (**2c**). The reaction was carried out for 5 h. Yield 120.3 mg (43%), grey powder, mp 71–72 °C. IR (ATR) ν 3071, 2909, 1669, 1557, 1341, 1267, 1078, 959. ¹H NMR (400 MHz, CDCl₃) δ 2.99 (6H, s, NMe₂), 4.75 (1H, d, *J* = 12.6 Hz, =CH(α)), 5.84 (1H, s), 6.84 (1H, s), 7.18 (1H, d, *J* = 12.6 Hz, =CH(β)). ¹⁹F NMR (376 MHz, CDCl₃) δ 90.2 (s, CF₃). ¹³C NMR (126 MHz, DMSO-*d*₆) δ 36.8 (br.s), 44.0 (br.s), 84.9, 103.5, 113.6 (q, *J* = 2.2 Hz, C-3), 118.7 (q, *J* = 273.2 Hz, CF₃), 147.6, 148.6 (q, *J* = 38.1 Hz, C-2), 166.9, 175.3. HRMS (ESI) *m/z* [M + H]⁺. Calculated for C₁₀H₁₁F₃NO₂: 234.0742. Found: 234.0735.

Methyl (*E*)-6-(2-(dimethylamino)vinyl)-4-oxo-4*H*-pyran-2-carboxylate (**2d**). The reaction was carried out for 6 h. Yield 72.3 mg (27%), yellow powder, mp 130–132 °C. IR (ATR) ν 3064, 2909, 1745, 1632, 1550, 1351, 1098, 959. ¹H NMR (500 MHz, CDCl₃) δ 2.97 (6H, s, NMe₂), 4.76 (1H, d, *J* = 13.0 Hz, =CH(α)), 5.89 (1H, d, *J* = 2.3 Hz, H-5), 6.88 (1H, d, *J* = 2.3 Hz, H-3), 7.32 (1H, d, *J* = 13.0 Hz, =CH(β)). ¹³C NMR (126 MHz, CDCl₃) δ 40.1 (br.s, NMe₂), 53.1, 86.9, 106.9, 118.7, 146.9, 150.0, 161.1, 166.8, 178.7. Anal. Calculated for C₁₁H₁₃NO₄: C 59.41; H 5.72; N 5.91. Found: C 59.19; H 5.87; N 6.27.

2-((*E*)-2-(Dimethylamino)vinyl)-6-((*E*)-styryl)-4*H*-pyran-4-one (**2e**). The reaction was carried out for 4 h. Yield 70.6 mg (22%), yellow powder, mp 75–77 °C. IR (ATR) ν 3055, 1642, 1610, 1524, 1397, 1157, 1103, 749. ¹H NMR (500 MHz, CDCl₃) δ 2.98 (6H, s, NMe₂), 4.79 (1H, d, *J* = 13.1 Hz, -CH=C-N), 5.84 (1H, d, *J* = 1.4 Hz, CH), 6.12 (1H, d, *J* = 1.4 Hz, CH), 6.66 (1H, d, *J* = 16.1 Hz, -CH=C-Ar), 7.24 (1H, d, *J* = 13.1 Hz, =CH-N), 7.27 (1H, d, *J* = 16.1 Hz, =CH-Ar), 7.39 (2H, t, *J* = 7.3 Hz, H-3, H-5 Ph), 7.51 (2H, d, *J* = 7.3 Hz, H-2, H-6 Ph). ¹³C NMR (126 MHz, CDCl₃) δ 40.8, 87.9, 105.6, 113.4, 120.6, 127.3, 128.9, 129.3, 134.1, 135.3, 145.5, 159.5, 165.7, 179.9. HRMS (ESI) *m/z* [M + H]⁺. Calculated for C₁₇H₁₈NO₂: 268.1338. Found: 268.1342.

2-((*E*)-4-(Dimethylamino)styryl)-6-((*E*)-2-(dimethylamino)vinyl)-4*H*-pyran-4-one (**2f**). The reaction was carried out for 3 h. Yield 268.2 mg (72%), brown crystals, mp 205–206 °C. IR (ATR) ν 2802, 1596, 1520, 1386, 1357, 1154, 1100. ¹H NMR (400 MHz, DMSO-*d*₆) δ 2.97 (12H, s, 2NMe₂), 4.87 (1H, d, *J* = 13.2 Hz, -CH=C-N), 5.65 (1H, d, *J* = 2.1 Hz, CH), 5.93 (1H, d, *J* = 2.1 Hz, CH), 6.69 (1H, d, *J* = 16.2 Hz, -CH=C-Ar), 6.73 (2H, d, *J* = 8.8 Hz, H-3, H-5 Ar), 7.36 (1H, d, *J* = 16.2 Hz, =CH-Ar), 7.48 (1H, d, *J* = 13.2 Hz, =CH-N), 7.53 (2H, d, *J* = 8.8 Hz, H-2, H-6 Ar). ¹³C NMR (101 MHz, DMSO-*d*₆) δ 39.7, 86.6, 103.8, 111.1, 111.9, 115.0, 122.9, 128.9, 134.2, 146.1, 150.9, 160.1, 165.2, 177.9 (NMe₂ was not observed). Anal. Calculated for C₁₉H₂₂N₂O₂: C 73.52; H 7.14; N 9.03. Found: C 73.47; H 7.27; N 9.10.

2-((*E*)-2-(Dimethylamino)vinyl)-6-((*E*)-4-methoxystyryl)-4*H*-pyran-4-one (**2g**). The reaction was carried out for 3 h. Yield 185.5 mg (51%), brown crystals, mp 155–157 °C. IR (ATR) ν 3070, 2967, 1637, 1612, 1549, 1383, 1346, 1096, 1020, 937. ¹H NMR (400 MHz, DMSO-*d*₆)

δ 2.96 (6H, s, 2NMe₂), 3.80 (3H, s, OMe), 4.88 (1H, d, J = 13.2 Hz, -CH=C-N), 5.67 (1H, d, J = 2.1 Hz, CH), 6.00 (1H, d, J = 2.1 Hz, CH), 6.85 (1H, d, J = 16.2 Hz, -CH=C-Ar), 6.99 (2H, d, J = 8.8 Hz, H-3, H-5, Ar), 7.43 (1H, d, J = 16.2 Hz, =CH-Ar), 7.51 (1H, d, J = 13.2 Hz, =CH-N), 7.65 (2H, d, J = 8.8 Hz, H-2, H-6, Ar). ¹³C NMR (101 MHz, DMSO-*d*₆) δ 55.2, 86.5, 103.9, 112.2, 114.3, 118.2, 128.1, 129.0, 133.4, 146.3, 159.5, 160.1, 165.4, 177.9 (the NMe₂ group was not observed). HRMS (ESI) m/z [M + H]⁺. Calculated for C₁₈H₂₀NO₃: 298.1443. Found: 298.1450.

3.3. Synthesis of Compounds 4

(*E*)-2-(2-(Dimethylamino)vinyl)-6-methyl-4H-pyran-4-one (**4a**). 2,6-Dimethyl-4-pyrone (**3a**) (0.202 g, 1.63 mmol), DMF-DMA (0.583 g, 4.89 mmol) and *N*-methylimidazole (66.9 mg, 0.815 mmol) were heated at 120 °C in an autoclave for 15 h. The reaction mixture was treated with boiling *n*-heptane (40 mL) to extract product **4a**. The residue was diluted with Et₂O to give 0.0876 g (23%) of brown needles of pyrone **5a** (mp 203–204 °C). The solution of *n*-heptane was evaporated to 2 mL, and the precipitate was filtered. Yield 0.0479 g (17%), yellow powder, mp 109–111 °C. IR (ATR) ν 3058, 2912, 1652, 1557, 1394, 1376, 1098, 913. ¹H NMR (400 MHz, CDCl₃) δ 2.21 (3H, s, Me), 2.91 (6H, s, NMe₂), 4.71 (1H, d, J = 13.2 Hz, =CH(α)), 5.75 (1H, d, J = 2.2 Hz, CH), 5.91 (1H, d, J = 2.2 Hz, CH), 7.12 (1H, d, J = 13.2 Hz, =CH(β)). ¹³C NMR (151 MHz, CDCl₃) δ 19.5, 86.8, 103.5, 112.5, 146.3, 163.2, 166.4, 178.5 (NMe₂ was not observed). The NMR spectra are in accordance with the literature data [13].

(*E*)-3-Bromo-2-(2-(dimethylamino)vinyl)-6-methyl-4H-pyran-4-one (**4b**). 2,6-Dimethyl-3-bromo-4-pyrone (**3b**) (100 mg, 0.493 mmol), DMF-DMA (70.6 mg, 0.592 mmol), and *N*-methylimidazole (60.8 mg, 0.740 mmol) were heated in an autoclave for 8 h at 120 °C. The reaction was monitored by TLC. After completion of the reaction (TLC monitoring), the product was filtered and washed with Et₂O (2 mL). The compound was further purified by column chromatography (CHCl₃:EtOH = 10:0.5). Yield 102 mg (80%), yellow powder, mp 162–163 °C. IR (ATR) ν 3063, 2918, 1661, 1558, 1421, 1270, 1007, 945, 773. ¹H NMR (500 MHz, CDCl₃) δ 2.23 (3H, s, Me), 3.01 (6H, s, NMe₂), 5.27 (1H, d, J = 13.0 Hz, =CH(α)), 6.00 (1H, s, H-5), 7.24 (1H, d, J = 13.0 Hz, =CH(β)). ¹³C NMR (126 MHz, CDCl₃) δ 19.3, 38.3, 44.0, 87.1, 103.1, 110.7, 147.2, 161.7, 162.8, 173.6. HRMS (ESI) m/z [M + H]⁺. Calculated for C₁₅H₁₆NO₂: 258.0085. Found: 258.0130.

3.4. General Method for the Synthesis of Bis(enamino)-substituted 4-Pyrones 5a,b

A mixture of 2,6-dimethyl-4-pyrone **3a** or **3b** (0.806 mmol), DMF-DMA (480 mg, 4.03 mmol), and *N*-methylimidazole (33.0 mg, 0.403 mmol) was heated in an autoclave for 15 h (for **5a**) or 10 h (for **5b**) at 130 °C. Then the reaction mixture was diluted with Et₂O (5 mL) and the product filtered.

2,6-Bis((*E*)-2-(dimethylamino)vinyl)-4H-pyran-4-one (**5a**). Yield 96.3 mg (51%), brown crystals, mp 203–204 °C. IR (ATR) ν 2990, 2810, 1640, 1615, 1542, 1360, 1335, 1095, 947. ¹H NMR (400 MHz, DMSO-*d*₆) δ 2.89 (12H, s, 2NMe₂), 4.75 (2H, d, J = 13.3 Hz, =CH(α)), 5.43 (2H, s, H-3, H-5), 7.29 (2H, d, J = 13.3 Hz, =CH(β)). ¹³C NMR (100 MHz, DMSO-*d*₆) δ 40.0–41.0 (br.s), 87.2, 103.2, 144.9, 163.5, 177.9. HRMS (ESI) m/z [M + H]⁺. Calculated for C₁₃H₁₉N₂O₂: 235.1447. Found: 235.1448.

3-Bromo-2,6-bis((*E*)-2-(dimethylamino)vinyl)-4H-pyran-4-one (**5b**). The product was additionally purified by column chromatography (CHCl₃:EtOH = 10:0.5). Yield 134 mg (53%), dark orange powder, mp 185–186 °C. IR (ATR) ν 3398, 3020, 2916, 1630, 1487, 1353, 1105, 947, 753. ¹H NMR (500 MHz, CDCl₃) δ 2.91 (6H, s, NMe₂), 2.97 (6H, s, NMe₂), 4.79 (1H, d, J = 13.2 Hz, CH(α)), 5.24 (1H, d, J = 13.0 Hz, =CH(α)), 5.75 (1H, s, H-5), 7.01 (1H, d, J = 13.2 Hz, CH(β)), 7.14 (1H, d, J = 13.0 Hz, =CH(β)). ¹³C NMR (126 MHz, CDCl₃) δ 40.7 (br.s, NMe₂), 87.6, 87.9, 102.1, 102.9, 144.7, 146.2, 160.5, 163.0, 173.6. HRMS (ESI) m/z [M + H]⁺. Calculated for C₁₅H₁₆NO₂: 313.0507. Found: 313.0550.

3.5. General Method for the Preparation of 2-((E)-4-Methoxystyryl)-6-((E)-2-aminovinyl)-4H-pyran-4-one **6a–c**

Enamino-substituted pyrone **2g** (75.7 mg, 0.255 mmol) and N-nucleophile (0.31 mmol) or *p*-phenylenediamine (13.7 mg, 0.127 mmol) were stirred at 90 °C for 3 h in AcOH (1 mL). For **6a,c**, the precipitate was filtered and washed with EtOH. For **6b**, the reaction mixture was diluted with H₂O (5 mL). The solid that formed was recrystallized from EtOH–toluene.

2-((E)-4-Methoxystyryl)-6-((E)-2-(phenylamino)vinyl)-4H-pyran-4-one (**6a**). Yield 75.6 mg (86%), yellow powder, mp 229–231 °C. IR (ATR) ν 3272, 3078, 2958, 1698, 2637, 1596, 1495, 1278, 1269. ¹H NMR (400 MHz, DMSO-*d*₆) δ 3.81 (3H, s, Me), 5.57 (1H, d, *J* = 13.3 Hz, =CH(α)), 5.99 (1H, d, *J* = 1.9 Hz, CH), 6.14 (1H, d, *J* = 1.9 Hz, CH), 6.92 (1H, d, *J* = 16.3 Hz, =CH(α')), 6.93 (1H, t, *J* = 7.7 Hz, H-4 Ph), 7.01 (2H, d, *J* = 7.9 Hz, H-3, H-5 Ar), 7.16 (2H, d, *J* = 7.9 Hz, H-2, H-6 Ph), 7.31 (2H, t, *J* = 7.8 Hz, H-3, H-5 Ph), 7.50 (1H, d, *J* = 16.3 Hz, =CH(β')), 7.66 (2H, d, *J* = 8.6 Hz, H-2, H-6 Ar), 7.92 (1H, t, *J* = 12.7 Hz, =CH(β)), 9.58 (1H, d, *J* = 12.2 Hz, NH). ¹³C NMR (100 MHz, DMSO-*d*₆) δ 55.7, 94.8, 107.0, 112.6, 114.9, 115.3, 118.5, 121.5, 128.5, 129.6, 129.9, 134.6, 136.3, 142.0, 160.8, 160.7, 164.4, 178.7. HRMS (ESI) *m/z* [M + H]⁺. Calculated for C₂₂H₂₀NO₃: 346.1456. Found: 346.3980.

2-((E)-2-(Diphenylamino)vinyl)-6-((E)-4-methoxystyryl)-4H-pyran-4-one (**6b**). Yield 88.1 mg (82%), yellow powder, mp 225–226 °C. IR (ATR) ν 3046, 3004, 2836, 1644, 1576, 1489, 1237, 1173. ¹H NMR (500 MHz, DMSO-*d*₆) δ 3.78 (3H, s, Me), 5.07 (1H, d, *J* = 13.5 Hz, =CH(α)), 5.92 (1H, s, CH), 6.14 (1H, s, CH), 6.92 (1H, d, *J* = 16.0 Hz, =CH(α')), 7.00 (2H, d, *J* = 7.9 Hz, H-3, H-5 Ar), 7.20 (4H, d, *J* = 7.5 Hz, H-2, H-6 Ph), 7.29 (2H, t, *J* = 7.1 Hz, H-4 Ph), 7.43 (1H, d, *J* = 16.0 Hz, =CH(β')), 7.48 (4H, t, *J* = 7.2 Hz, H-3, H-5 Ph), 7.60 (2H, d, *J* = 8.6, H-2, H-6 Ar), 8.09 (1H, d, *J* = 13.5 Hz, =CH(β)). ¹³C NMR (125 MHz, DMSO-*d*₆) δ 55.3, 97.0, 107.7, 112.0, 114.3, 117.9, 123.8, 125.6, 127.9, 129.0, 129.9, 134.3, 139.5, 145.5, 160.2, 160.3, 163.2, 178.2. HRMS (ESI) *m/z* [M + H]⁺. Calculated for C₂₈H₂₄NO₃: 422.1756. Found: 422.1747.

6,6'-((1E,1'E)-(1,4-Phenylenebis(azanediyl))bis(ethene-2,1-diyl))bis(2-((E)-4-methoxystyryl)-4H-pyran-4-one) (**6c**). Yield 63.5 mg (82%), burgundy powder, mp 204–205 °C. IR (ATR) ν 3040, 2934, 2839, 1637, 1504, 1396, 1253, 1152. ¹H NMR (500 MHz, DMSO-*d*₆) δ 3.78 (6H, s, 2Me), 5.52 (2H, d, *J* = 13.1 Hz, =CH(α)), 5.95 (2H, d, *J* = 2.1 Hz, CH), 6.12 (2H, d, *J* = 2.1 Hz, CH), 6.92 (2H, d, *J* = 16.2 Hz, =CH(α')), 6.97 (4H, d, *J* = 8.6 Hz, H-3, H-5 Ar), 7.15 (4H, s, Ar), 7.49 (2H, d, *J* = 16.2 Hz, =CH(β')), 7.66 (4H, d, *J* = 8.6 Hz, H-2, H-6 Ar), 7.87 (2H, t, *J* = 12.0 Hz, =CH(β)), 9.52 (2H, d, *J* = 12.0 Hz, NH). ¹³C NMR (100 MHz, DMSO-*d*₆) δ 55.7, 106.4, 112.6, 114.8, 116.9, 118.6, 128.5, 129.6, 136.3, 160.7, 164.7, 172.4, 178.6. HRMS (ESI) *m/z* [M + H]⁺. Calculated for C₃₈H₃₃N₂O₆: 613.2339. Found: 613.6820.

2-((E)-2-(Benzylamino)vinyl)-6-((E)-4-methoxystyryl)-4H-pyran-4-one (**6d**). Enamino-substituted pyrone **2g** (75.7 mg, 0.255 mmol) and benzylamine (32.8 mg, 0.306 mmol) were refluxed for 7 h in MeCN (1 mL). The reaction mixture was diluted with H₂O (5 mL). The solid that formed was filtered and recrystallized from hexane–toluene. Yield 69.7 mg (76%), yellow powder, mp 144–145 °C. IR (ATR) ν 2900, 1651, 1520, 1394, 1250, 1169, 1027. ¹H NMR (400 MHz, DMSO-*d*₆) δ 3.80 (3H, s, Me), 4.33 (2H, d, *J* = 5.3 Hz, CH₂), 5.04 (1H, d, *J* = 13.4 Hz, =CH(α)), 5.66 (1H, s, *J* = 2.2 Hz, CH), 6.00 (1H, s, *J* = 2.2 Hz, CH), 6.85 (2H, d, *J* = 16.2 Hz, =CH(α')), 6.99 (2H, d, *J* = 8.7 Hz, H-3, H-5 Ar), 7.25–7.31 (1H, m, Ph), 7.31–7.40 (6H, m), 7.43 (1H, br.s, NH), 7.61 (2H, d, *J* = 8.7 Hz, H-2, H-6 Ar). ¹³C NMR (101 MHz, DMSO-*d*₆) δ 31.1, 55.7, 87.5, 104.9, 112.7, 114.8, 118.8, 127.6, 127.8, 128.5, 128.9, 129.5, 133.7, 159.9, 160.6, 165.8, 178.5. HRMS (ESI) *m/z* [M + H]⁺. Calculated for C₂₂H₂₀NO₃: 346.1456. Found: 346.3980.

2,6-Bis((E)-2-(phenylamino)vinyl)-4H-pyran-4-one (**6e**). Pyrone **5a** (100 mg, 0.427 mmol) and aniline (99.4 g, 1.07 mmol) were stirred at room temperature for 24 h in AcOH (1.5 mL). The precipitate was filtered and washed with EtOH. Yield 77.5 mg (55%), orange powder, mp 217–218 °C. IR (ATR) ν 3221, 3054, 1657, 1645, 1544, 1493, 1278, 1148, 945. ¹H NMR (500 MHz, DMSO-*d*₆) δ 5.52 (2H, d, *J* = 13.3 Hz, =CH(α)), 5.77 (2H, s, CH), 6.92 (2H, t, *J* = 7.3 Hz, H-2, H-6 Ph), 7.13 (4H, d, *J* = 7.9 Hz, H-3, H-5 Ph), 7.87 (2H, t, *J* = 12.8 Hz, =CH(β)), 9.49 (2H, d, *J* = 12.3 Hz, NH). ¹³C NMR (126 MHz, DMSO-*d*₆) δ 94.4, 106.0, 114.6,

120.8, 129.4, 135.2, 141.9, 162.5, 178.2. Anal. Calculated for C₂₁H₁₈N₂O₂: C 76.34; H 5.49; N 8.48. Found: C 76.42; H 5.56; N 8.43.

3.6. Synthesis of Compounds 7a,b

2-((*E*)-4-Methoxystyryl)-6-((*E*)-2-(2-methyl-1H-indol-3-yl)vinyl)-4H-pyran-4-one (7a). Styryl-4-pyrone 2g (105 mg, 0.353 mmol) and 2-methylindole (55.6 mg, 0.424 mmol) were refluxed in AcOH (1 mL) for 7 h. The precipitate formed was filtered and washed with EtOH. Yield 0.0835 g (62%), yellow powder, mp 284–285 °C. IR (ATR) ν 3131, 3035, 2958, 2928, 2834, 1604, 1556, 1394. ¹H NMR (400 MHz, DMSO-*d*₆) δ 2.63 (3H, s, Me), 3.82 (3H, s, OMe), 6.25 (1H, d, *J* = 2.2 Hz, CH), 6.37 (1H, d, *J* = 2.2 Hz, CH), 6.85 (1H, d, *J* = 16.2 Hz, =CH(α)), 7.00 (1H, d, *J* = 16.2 Hz, =CH(α)), 7.03 (2H, d, *J* = 8.9 Hz, H-3, H-5, Ar), 7.12–7.19 (2H, m, H-5, H-6 Ind), 7.35–7.42 (1H, m, H-7 Ind), 7.58 (1H, d, *J* = 16.1 Hz, =CH(β)), 7.68 (2H, d, *J* = 8.7 Hz, H-2, H-6 Ar), 7.79 (1H, d, *J* = 16.2 Hz, =CH(β)), 7.98–8.04 (1H, m, H-4 Ind), 11.65 (1H, s, NH). ¹³C NMR (151 MHz, DMSO-*d*₆) δ 12.2, 55.8, 109.4, 111.0, 111.8, 113.1, 113.2, 115.0, 118.5, 120.1, 121.0, 122.2, 126.2, 128.4, 129.7, 135.2, 136.5, 141.4, 161.0, 161.3, 163.3, 179.3. HRMS (ESI) *m/z* [M + H]⁺. Calculated for C₁₇H₁₈NO₂: 268.1338. Found: 268.1342.

2,6-Bis((*E*)-2-(2-methyl-1H-indol-3-yl)vinyl)-4H-pyran-4-one (7b). Bis(enamino)-substituted 4-pyrone 5a (100 mg, 0.353 mmol) and 2-methylindole (55.6 mg, 0.424 mmol) was refluxed in AcOH (1 mL) for 10 h. The precipitate formed was filtered and washed with EtOH. Yield 74.6 mg (52%), orange powder, mp >270 °C. IR (ATR) ν 3178, 3056, 1631, 1611, 1539, 1399, 1274, 1153, 936. ¹H NMR (500 MHz, DMSO-*d*₆) δ 2.64 (6H, s, 2Me), 6.28 (2H, s, H-3, H-5), 6.87 (2H, d, *J* = 16.1 Hz, =CH(α)), 7.13–7.19 (4H, m, H-5, H-6 Ind), 7.36–7.41 (2H, m, H-7 Ind), 7.82 (2H, d, *J* = 16.1 Hz, =CH(β)), 7.98–8.04 (2H, m, H-4 Ind), 11.7 (2H, s, NH). ¹³C NMR (126 MHz, DMSO-*d*₆) δ 11.6, 108.8, 110.7, 111.3, 112.8, 119.6, 120.5, 121.7, 125.6, 128.4, 136.0, 140.7, 162.1, 179.0. HRMS (ESI) *m/z* [M + H]⁺. Calculated for C₂₅H₂₂NO₃: 384.1600. Found: 384.1608.

3.7. Synthesis of 6-(3-Phenylisoxazol-4-yl)-4H-pyran-4-ones 8a,b

2-((Dimethylamino)vinyl)-6-styryl-4H-pyran-4-one 2f,g (0.32 mmol) and *N*-hydroxybenzimidoyl chloride (60.7 mg, 0.390 mmol) were stirred for 4 days in dry 1,4-dioxane at room temperature. The precipitate that formed was filtered and washed with toluene.

(*E*)-2-(4-(Dimethylamino)styryl)-6-(3-phenylisoxazol-4-yl)-4H-pyran-4-one (8a). Yield 81.2 mg (66%), brown crystals, mp 199–200 °C. IR (ATR) ν 3078, 2909, 1587, 1523, 1350, 1127, 940. ¹H NMR (400 MHz, DMSO-*d*₆) δ 2.97 (6H, s, NMe₂), 6.20 (1H, s, CH), 6.33–6.48 (2H, m), 6.65 (1H, d, *J* = 16.5 Hz, =CH(β)), 6.70 (2H, d, *J* = 7.6 Hz, Ar), 7.24 (2H, d, *J* = 7.6, Ar), 7.47–7.71 (5H, m, Ph), 9.82 (1H, s, H-5 Isox). ¹³C NMR (100 MHz, DMSO-*d*₆) δ 112.3, 113.4, 113.7, 114.0, 122.7, 128.2, 129.2, 129.4, 129.5, 130.8, 136.3, 151.7, 154.7, 159.9, 162.2, 162.9, 178.5 (NMe₂ + 1C were not observed). HRMS (ESI) *m/z* [M + H]⁺. Calculated for C₂₄H₂₁N₂O₃: 388.1522. Found: 388.1524.

(*E*)-2-(4-Methoxystyryl)-6-(3-phenylisoxazol-4-yl)-4H-pyran-4-one (8b). Yield 95.1 mg (80%), light yellow crystals, mp 221–222 °C. IR (ATR) ν 3048, 2837, 1657, 1626, 1512, 1379, 823. ¹H NMR (400 MHz, DMSO-*d*₆) δ 3.80 (3H, s, OMe), 6.27 (1H, s, CH), 6.42 (1H, s, CH), 6.46 (1H, d, *J* = 15.3 Hz, =CH(α)), 6.83 (1H, d, *J* = 15.3 Hz, =CH(β)), 6.97 (2H, br.s, Ar), 7.37 (2H, br.s, Ar), 7.45–7.78 (5H, m, Ph), 9.82 (1H, s, H-5 Isox). ¹³C NMR (126 MHz, DMSO-*d*₆) δ 54.9, 112.5, 113.0, 113.3, 114.5, 127.3, 128.2, 128.5, 128.9, 129.7, 130.3, 154.8, 157.9, 169.1, 161.1, 166.4, 177.4 (2C were not observed). Anal. Calculated for C₂₇H₁₇NO₄: C 74.38; H 4.61; N 3.77. Found: C 74.15; H 4.56; N 3.69.

3.8. Synthesis of compound 9

2,6-Bis(3-phenylisoxazol-4-yl)-4H-pyran-4-one (9). Bis(enamino)-substituted pyrone 5a (100 mg, 0.427 mmol) and *N*-hydroxybenzimidoyl chloride (146 mg, 0.938 mmol) were refluxed in dry dioxane (2 mL) for 4 h. The precipitate formed was filtered and washed with EtOH. Yield 64.0 mg (39%), beige powder, mp 238–239 °C. IR (ATR) ν 3066, 2890, 1657, 1612, 1549, 1445, 1404, 1143, 913. ¹H NMR (500 MHz, DMSO-*d*₆) δ 6.19 (2H, s, H-3, H-5), 7.51–7.55

(m, 8H, Ph); 7.55–7.60 (m, 2H, Ph), 9.13 (s, 2H, Isox). ^{13}C NMR (126 MHz, DMSO- d_6) δ 112.5, 113.1, 127.1, 128.6, 128.9, 130.3, 155.1, 159.1, 161.3, 177.0. Anal. Calculated for $\text{C}_{23}\text{H}_{14}\text{N}_2\text{O}_4$: C 72.25; H 3.69; N 7.33. Found: C 72.13; H 3.84; N 7.45.

Supplementary Materials: The following supporting information can be downloaded at: <https://www.mdpi.com/xxx/s1>; Table S1: ground state frontier orbitals for compounds **4a** and **5a** in vacuo; Table S2: Ground state frontier orbitals for compounds **4a** and **5a** in DMSO; Table S3: ground state frontier orbitals for compounds **4a** and **5a** in ethanol; Table S4: ground state frontier orbitals for compounds **4a** and **5a** in methanol; Table S5: frontier orbitals of the first singlet excited state for the relaxed geometry of compounds **4a** and **5a** in vacuo; Table S6: frontier orbitals of the first singlet excited state for the relaxed geometry of compounds **4a** and **5a** in DMSO; Table S7: frontier orbitals of the first singlet-excited state for the relaxed geometry of compounds **4a** and **5a** in ethanol; Table S8: frontier orbitals of the first singlet-excited state for the relaxed geometry of compounds **4a** and **5a** in methanol; calculated normalized UV-vis spectra for compounds **4a** and **5a** in DMSO, methanol, and ethanol; electron density difference maps for compounds **4a** and **5a**; the method of preparation of 2-methyl-6-trifluoromethyl-4-pyrone; full ^1H , ^{19}F , and ^{13}C NMR spectra of all synthesized compounds; Figure S1: Normalized absorption and emission spectra of **4a** in DMSO at a CAM-B3LYP level; Figure S2: Normalized absorption and emission spectra of **4a** in ethanol at a CAM-B3LYP level; Figure S3: Normalized absorption and emission spectra of **4a** in methanol at a CAM-B3LYP level; Figure S4: Normalized absorption and emission spectra of **5a** in DMSO at a CAM-B3LYP level; Figure S5: Normalized absorption and emission spectra of **5a** in ethanol at a CAM-B3LYP level; Figure S6: Normalized absorption and emission spectra of **5a** in methanol at a CAM-B3LYP level; Figure S7: An electron density difference map for the $\text{S}_0 \rightarrow \text{S}_1$ transition of compound **4a** in vacuo; Figure S8: An electron density difference map for the $\text{S}_0 \rightarrow \text{S}_1$ transition of compound **4a** in methanol; Figure S9: An electron density difference map for the $\text{S}_0 \rightarrow \text{S}_1$ transition of compound **5a** in vacuo; Figure S10: An electron density difference map for the $\text{S}_0 \rightarrow \text{S}_1$ transition of compound **5a** in methanol.

Author Contributions: Conceptualization and methodology were provided by V.Y.S. and D.L.O.; D.L.O. conceived and designed the experiments. The experimental work was conducted by D.I.N., O.E.M., A.S.S., V.V.F., S.A.U. and A.E.S.; A.E.S. carried out photophysical experiments. D.L.O. and A.E.S. analyzed the results. D.L.O. studied and systemized the spectral data. Theoretical calculation was carried out by M.Y.K. D.L.O., M.Y.K. and V.Y.S. wrote the paper. Project administration and funding acquisition were carried out by V.Y.S. and D.L.O. All authors have read and agreed to the published version of the manuscript.

Funding: This research was funded by the Russian Science Foundation, grant number 18-13-00186 (<https://rscf.ru/project/18-13-00186/> (accessed on 12 December 2022)).

Institutional Review Board Statement: Not applicable.

Informed Consent Statement: Not applicable.

Data Availability Statement: Data is contained within the article and Supplementary Materials.

Acknowledgments: Analytical studies were carried out using equipment at the Center for Joint Use ‘Spectroscopy and Analysis of Organic Compounds’ at the Postovsky Institute of Organic Synthesis of the Russian Academy of Sciences (Ural Branch) and the Laboratory of Complex Investigations and Expert Evaluation of Organic Materials of the Center for Joint Use at the Ural Federal University.

Conflicts of Interest: The authors declare no conflict of interest.

Sample Availability: Samples of the compounds are not available from the authors.

References

1. Singh, K.S. Pyrone-derived marine natural products: A review on isolation, bio-activities and synthesis. *Curr. Org. Chem.* **2020**, *24*, 354–401. [[CrossRef](#)]
2. Ishibashi, Y.; Ohba, S.; Nishiyama, S.; Yamamura, S. Total synthesis of phenoxan and a related pyrone derivative. *Tetrahedron Lett.* **1996**, *37*, 2997–3000. [[CrossRef](#)]

3. Schiavone, D.V.; Kapkayeva, D.M.; Murelli, R.P. Investigations into a stoichiometrically equivalent intermolecular oxidopyrylium [5 + 2] cycloaddition reaction leveraging 3-hydroxy-4-pyrone-based oxidopyrylium dimers. *J. Org. Chem.* **2021**, *86*, 3826–3835. [[CrossRef](#)]
4. Usachev, S.A.; Nigmatova, D.I.; Mysik, D.K.; Naumov, N.A.; Obydenov, D.L.; Sosnovskikh, V.Y. 2-Aryl-6-polyfluoroalkyl-4-pyrones as promising R^F-building-blocks: Synthesis and application for construction of fluorinated azaheterocycles. *Molecules* **2021**, *26*, 4415. [[CrossRef](#)] [[PubMed](#)]
5. Milyutin, C.V.; Komogortsev, A.N.; Lichitsky, B.V.; Melekhina, V.G.; Minyaev, M.E. Construction of spiro- γ -butyrolactone core via cascade photochemical reaction of 3-hydroxypyran-4-one derivatives. *Org. Lett.* **2021**, *23*, 5266–5270. [[CrossRef](#)]
6. Chen, J.; Wu, L.; Wu, J. Kojic acid and maltol: The “transformers” in organic synthesis. *Chin. Chem. Lett.* **2020**, *31*, 2993–2995. [[CrossRef](#)]
7. Yasukata, T.; Masui, M.; Ikarashi, F.; Okamoto, K.; Kurita, T.; Nagai, M.; Sugata, Y.; Miyake, N.; Hara, S.; Adachi, Y.; et al. Practical synthetic method for the preparation of pyrone diesters: An efficient synthetic route for the synthesis of dolutegravir sodium. *Org. Process Res. Dev.* **2019**, *23*, 565–570. [[CrossRef](#)]
8. Obydenov, D.L.; Khammatova, L.R.; Eltsov, O.S.; Sosnovskikh, V.Y. A chemo- and regiocontrolled approach to bipyrazoles and pyridones via the reaction of ethyl 5-acyl-4-pyrone-2-carboxylates with hydrazines. *Org. Biomol. Chem.* **2018**, *16*, 1692–1707. [[CrossRef](#)]
9. Palkina, K.A.; Ipatova, D.A.; Shakhova, E.S.; Balakireva, A.V.; Markina, N.M. Therapeutic potential of hispidin—Fungal and plant polyketide. *J. Fungi* **2021**, *7*, 323. [[CrossRef](#)]
10. Purtov, K.V.; Petushkov, V.N.; Baranov, M.S.; Mineev, K.S.; Rodionova, N.S.; Kaskova, Z.M.; Tsarkova, A.S.; Petunin, A.I.; Bondar, V.S.; Rodicheva, E.K.; et al. The chemical basis of fungal bioluminescence. *Angew. Chem. Int. Ed.* **2015**, *54*, 8124–8128. [[CrossRef](#)]
11. Zuidema, D.R.; Jones, P.B. Triplet photosensitization in cyercene A and related pyrones. *J. Photochem. Photobiol. B Biol.* **2006**, *83*, 137–145. [[CrossRef](#)] [[PubMed](#)]
12. Moses, J.E.; Baldwin, J.E.; Adlington, R.M. An efficient synthesis of cyercene A. *Tetrahedron Lett.* **2004**, *45*, 6447–6448. [[CrossRef](#)]
13. Krasnaya, Z.A.; Smirnova, Y.V.; Tatikolov, A.S.; Kuz'min, V.A. Synthesis and photonics of ketocyanine dyes, 2,6-bis(4-dimethylaminoalka-1,3-dienyl)-4H-pyran-4-ones and ethoxytridecamethine salts based on them. *Russ. Chem. Bull.* **1999**, *48*, 1329–1334. [[CrossRef](#)]
14. Obydenov, D.L.; Simbirtseva, A.E.; Sosnovskikh, V.Y. Synthesis of 4-oxo-6-styryl-4H-pyran-2-carbonitriles and their application for the construction of new 4-pyrone derivatives. *Res. Chem. Intermed.* **2022**, *48*, 2155–2179. [[CrossRef](#)]
15. Rahimpour, K.; Zarenezhad, H.; Teimuri-Mofrad, R. Transition metal-catalyzed C–N cross-coupling reaction of bromine-substituted pyranilidene derivatives: Synthesis, characterization, and optical properties study of pyran-based chromophores. *J. Iran. Chem. Soc.* **2020**, *17*, 2627–2636. [[CrossRef](#)]
16. Cao, Y.; Xi, Y.; Teng, X.; Li, Y.; Yan, X.; Chen, L. Alkoxy substituted D-p-A dimethyl-4-pyrone derivatives: Aggregation induced emission enhancement, mechanochromic and solvatochromic properties. *Dyes Pigm.* **2017**, *137*, 75–83. [[CrossRef](#)]
17. Cao, Y.; Chen, L.; Xi, Y.; Li, Y.; Yan, X. Stimuli-responsive 2,6-diarylethene-4H-pyran-4-one derivatives: Aggregation induced emission enhancement, mechanochromism and solvatochromism. *Mater. Lett.* **2018**, *212*, 225–230. [[CrossRef](#)]
18. Liu, D.; Cao, Y.; Yan, X.; Wang, B. Two stimulus responsive carbazole substituted D- π -A pyrone compounds exhibiting mechanochromism and solvatochromism. *Res. Chem. Intermed.* **2019**, *45*, 2429–2439. [[CrossRef](#)]
19. Pecourneau, J.; Losantos, R.; Monari, A.; Parant, S.; Pasc, A.; Mourer, M. Synthesis and photoswitching properties of bioinspired dissymmetric γ -pyrone, an analogue of cyclocurcumin. *J. Org. Chem.* **2021**, *86*, 8112–8126. [[CrossRef](#)]
20. Guo, Z.; Zhu, W.; Tian, H. Dicyanomethylene-4H-pyranchromophores for OLED emitters, logic gates and optical chemosensors. *Chem. Commun.* **2012**, *48*, 6073–6084. [[CrossRef](#)]
21. Casimiro, L.; Maisonneuve, S.; Retailleau, P.; Silvi, S.; Xie, J.; Métivier, R. Photophysical properties of 4-dicyanomethylene-2-methyl-6-(*p*-dimethylamino-styryl)-4H-pyran revisited: Fluorescence versus photoisomerization. *Chem. Eur. J.* **2020**, *26*, 14341–14350. [[CrossRef](#)] [[PubMed](#)]
22. Hoche, J.; Schulz, A.; Dietrich, L.M.; Humeniuk, A.; Stolte, M.; Schmidt, D.; Brixner, T.; Würthner, F.; Mitric, R. The origin of the solvent dependence of fluorescence quantum yields in dipolar merocyanine dyes. *Chem. Sci.* **2019**, *10*, 11013–11022. [[CrossRef](#)] [[PubMed](#)]
23. Gao, M.-J.; Hua, Y.; Xu, J.-Q.; Zhang, L.-X.; Wang, S.; Kang, Y.-F. Near-infrared fluorescence probe with a large Stokes shift for selectively imaging of hydrogen peroxide in living cells and in vivo. *Dyes Pigm.* **2022**, *197*, 109930. [[CrossRef](#)]
24. Krasnaya, Z.A.; Smirnova, Y.V.; Shvedova, L.A.; Tatikolov, A.S.; Kuz'min, V.A. Synthesis and spectroscopic properties of cross-conjugated ketones and meso-substituted tridecamethine salts containing the pyran or pyridone fragment. *Russ. Chem. Bull.* **2003**, *52*, 2029–2037. [[CrossRef](#)]
25. Obydenov, D.L.; Simbirtseva, A.E.; Piksin, S.E.; Sosnovskikh, V.Y. 2,6-Dicyano-4-pyrone as a novel and multifarious building block for the synthesis of 2,6-bis(hetaryl)-4-pyrones and 2,6-bis(hetaryl)-4-pyridinols. *ACS Omega* **2020**, *5*, 33406–33420. [[CrossRef](#)]
26. Obydenov, D.L.; Usachev, B.I.; Sosnovskikh, V.Y. Reactions of 2-mono- and 2,6-disubstituted 4-pyrones with phenylhydrazine as general method for the synthesis of 3-(*N*-phenylpyrazolyl)indoles. *Chem. Heterocycl. Compd.* **2015**, *50*, 1388–1403. [[CrossRef](#)]
27. Usachev, B. 2-(Trifluoromethyl)-4H-pyran-4-ones: Convenient, available and versatile building-blocks for regioselective syntheses of trifluoromethylated organic compounds. *J. Fluor. Chem.* **2015**, *172*, 80–91. [[CrossRef](#)]

28. Zatsikha, Y.V.; Yakubovskiy, V.P.; Shandura, M.P.; Kovtun, Y.P. Functionalized bispyridoneannulated BODIPY—Bright long-wavelength fluorophores. *Dyes Pigm.* **2015**, *114*, 215–221. [[CrossRef](#)]
29. Bosson, J.; Labrador, G.M.; Besnard, C.; Jacquemin, D.; Lacour, J. Chiral near-infrared fluorophores by self-promoted oxidative coupling of cationic helicenes with amines/enamines. *Angew. Chem.* **2021**, *133*, 8815–8820. [[CrossRef](#)]
30. Wang, D.; Guo, X.; Wu, H.; Wu, Q.; Wang, H.; Zhang, X.; Hao, E.; Jiao, L. Visible light excitation of BODIPYs enables dehydrogenative enamination at their α -positions with aliphatic amines. *J. Org. Chem.* **2020**, *85*, 8360–8370. [[CrossRef](#)]
31. Baleeva, N.S.; Zaitseva, S.O.; Mineev, K.S.; Khavroshechkina, A.V.; Zagudaylova, M.B.; Baranov, M.S. Enamine–azide [2+3]-cycloaddition as a method to introduce functional groups into fluorescent dyes. *Tetrahedron Lett.* **2019**, *60*, 456–459. [[CrossRef](#)]
32. Lugovik, K.I.; Popova, A.V.; Eltyshev, A.K.; Benassi, E.; Belskaya, N.P. Synthesis of thiazoles bearing aryl enamine/aza-enamine side chains: Effect of the π -conjugated spacer structure and hydrogen bonding on photophysical properties. *Eur. J. Org. Chem.* **2017**, *2017*, 4175–4187. [[CrossRef](#)]
33. Stanovnik, B.; Svete, J. Synthesis of heterocycles from alkyl 3-(dimethylamino)propenoates and related enamines. *Chem. Rev.* **2004**, *104*, 2433–2480. [[CrossRef](#)]
34. Ghosh, C.K.; Bhattacharyya, S.; Ghosh, C.; Patra, A. Benzopyrans. Part 41. Reactions of 2-(2-dimethylaminovinyl)-1-benzopyran-4-ones with various dienophiles. *J. Chem. Soc. Perkin Trans.* **1999**, *1*, 3005–3013. [[CrossRef](#)]
35. Gümüş, M.; Koca, İ. Enamines and dimethylamino imines as building blocks in heterocyclic synthesis: Reactions of DMF-DMA reagent with different functional groups. *Chemistryselect* **2020**, *5*, 12377–12397. [[CrossRef](#)]
36. Beliaev, N.A.; Shafikov, M.Z.; Efimov, I.V.; Beryozkina, T.V.; Lubec, G.; Dehaen, W.; Bakulev, V.A. Design and synthesis of imidazoles linearly connected to carbocyclic and heterocyclic rings via a 1,2,3-triazole linker. Reactivity of β -azolyl enamines towards heteroaromatic azides. *New J. Chem.* **2018**, *42*, 7049–7059. [[CrossRef](#)]
37. Brouwer, A.M. Standards for photoluminescence quantum yield measurements in solution (IUPAC Technical Report). *Pure Appl. Chem.* **2011**, *83*, 2213–2228. [[CrossRef](#)]
38. Fabian, J. TDDFT-calculations of Vis/NIR absorbing compounds. *Dyes Pigm.* **2010**, *84*, 36–53. [[CrossRef](#)]
39. Chipem, F.A.S.; Mishra, A.; Krishnamoorthy, G. The role of hydrogen bonding in excited state intramolecular charge transfer. *Phys. Chem. Chem. Phys.* **2012**, *14*, 8775–8790. [[CrossRef](#)]
40. Clark, B.P.; Ross, W.J.; Todd, A. 6-Substituted Pyranone Compounds and Their Use as Pharmaceuticals. U.S. Patent 4471129, 30 July 1984.
41. Coffin, A.; Ready, J.M. Selective synthesis of (+)-dysoline. *Org. Lett.* **2019**, *21*, 648–651. [[CrossRef](#)]
42. Chen, C.H.; Klubek, K.P.; Shi, J. Red Organic Electroluminescent Materials. U.S. Patent 5908581, 1 June 1999.
43. Becke, A.D. Density-functional thermochemistry. III. The role of exact exchange. *J. Chem. Phys.* **1993**, *98*, 5648–5652. [[CrossRef](#)]
44. Marenich, A.V.; Cramer, C.J.; Truhlar, D.G. Universal solvation model based on solute electron density and on a continuum model of the solvent defined by the bulk dielectric constant and atomic surface tensions. *J. Phys. Chem. B* **2009**, *113*, 6378–6396. [[CrossRef](#)] [[PubMed](#)]
45. Yanai, T.; Tew, D.P.; Handy, N.C. A new hybrid exchange–correlation functional using the Coulomb-attenuating method (CAM-B3LYP). *Chem. Phys. Lett.* **2004**, *393*, 51–57. [[CrossRef](#)]
46. Parthasarathy, V.; Castet, F.; Pandey, R.; Mongin, O.; Das, P.K.; Blanchard-Desce, M. Unprecedented intramolecular cyclization in strongly dipolar extended merocyanine dyes: A route to novel dyes with improved transparency, nonlinear optical properties and thermal stability. *Dyes Pigm.* **2016**, *130*, 70–78. [[CrossRef](#)]
47. Barca, G.M.J.; Bertoni, C.; Carrington, L.; Datta, D.; De Silva, N.; Deustua, J.E.; Fedorov, D.G.; Gour, J.R.; Gunina, A.O.; Guidez, E.; et al. Recent developments in the general atomic and molecular electronic structure system. *J. Chem. Phys.* **2020**, *152*, 154102. [[CrossRef](#)]
48. Bode, B.M.; Gordon, M.S. Macmolplt: A graphical user interface for GAMESS. *J. Mol. Graph. Model.* **1998**, *16*, 133–138. [[CrossRef](#)] [[PubMed](#)]
49. Lu, T.; Chen, F. Multiwfn: A multifunctional wavefunction analyzer. *J. Comput. Chem.* **2012**, *33*, 580–592. [[CrossRef](#)] [[PubMed](#)]